Title

Intercellular Arc Signaling Regulates Vasodilation.

Authors

de la Peña, June Bryan
Barragan-Iglesias, Paulino
Lou, Tzu-Fang
et al.

Cellular/Molecular

Intercellular Arc Signaling Regulates Vasodilation

June Bryan de la Peña,[1]* Paulino Barragan-Iglesias,[2,3]* Tzu-Fang Lou,[1]* Nikesh Kunder,[1] Sarah Loerch,[4] Tarjani Shukla,[1] Lokesh Basavarajappa,[5] Jane Song,[1,5] Dominique N. James,[5] Salim Megat,[2] Jamie K. Moy,[2] Andi Wanghzou,[2] Pradipta R. Ray,[2] Kenneth Hoyt,[5] Oswald Steward,[6] Theodore J. Price,[2,7] Jason Shepherd,[8] and Zachary T. Campbell[1,7]

[1]Department of Biological Sciences, University of Texas at Dallas, Richardson, Texas 75080, [2]University of Texas at Dallas, School of Behavioral and Brain Sciences, Richardson, Texas 75080, [3]Department of Physiology and Pharmacology, Center for Basic Sciences, Autonomous University of Aguascalientes, Aguascalientes 20131, Mexico, [4]Janelia Research Campus, Howard Hughes Medical Institute, Ashburn, Virginia 20147, [5]Department of Bioengineering, University of Texas at Dallas, Richardson, Texas 75080, [6]Reeve-Irvine Research Center, Departments of Anatomy and Neurobiology, Neurobiology and Behavior, Neurosurgery, School of Medicine, University of California Irvine, Irvine, California 92697, [7]Center for Advanced Pain Studies, University of Texas at Dallas, Richardson, Texas 75080, and [8]Department of Neurobiology and Anatomy, University of Utah, Salt Lake City, Utah 84112

Injury responses require communication between different cell types in the skin. Sensory neurons contribute to inflammation and can secrete signaling molecules that affect non-neuronal cells. Despite the pervasive role of translational regulation in nociception, the contribution of activity-dependent protein synthesis to inflammation is not well understood. To address this problem, we examined the landscape of nascent translation in murine dorsal root ganglion (DRG) neurons treated with inflammatory mediators using ribosome profiling. We identified the activity-dependent gene, Arc, as a target of translation in vitro and in vivo. Inflammatory cues promote local translation of Arc in the skin. Arc-deficient male mice display exaggerated paw temperatures and vasodilation in response to an inflammatory challenge. Since Arc has recently been shown to be released from neurons in extracellular vesicles (EVs), we hypothesized that intercellular Arc signaling regulates the inflammatory response in skin. We found that the excessive thermal responses and vasodilation observed in Arc defective mice are rescued by injection of Arc-containing EVs into the skin. Our findings suggest that activity-dependent production of Arc in afferent fibers regulates neurogenic inflammation potentially through intercellular signaling.

Key words: Arc; DRG; neuroinflamation; nociceptors; translational control

Significance Statement

Nociceptors play prominent roles in pain and inflammation. We examined rapid changes in the landscape of nascent translation in cultured dorsal root ganglia (DRGs) treated with a combination of inflammatory mediators using ribosome profiling. We identified several hundred transcripts subject to rapid preferential translation. Among them is the immediate early gene (IEG) Arc. We provide evidence that Arc is translated in afferent fibers in the skin. Arc-deficient mice display several signs of exaggerated inflammation which is normalized on injection of Arc containing extracellular vesicles (EVs). Our work suggests that noxious cues can trigger Arc production by nociceptors which in turn constrains neurogenic inflammation in the skin.

Introduction

The skin forms a protective barrier to pathogens and is an essential point of contact between vertebrates and their environment. Skin is the single largest sensory organ because of innervation by nerve fibers that detect a broad range of stimuli. Sensory fibers communicate information from the periphery to the central nervous system. These cues can elicit behavioral responses that promote injury avoidance. A second critical function enabled by sensory neurons is regulated release of signaling molecules that influence blood flow, cellular proliferation, and immune response (Toda et al., 2008; Dubin and Patapoutian, 2010; Pinho-Ribeiro et al., 2017). While a handful of the factors released by afferent fibers have been identified, the mechanisms that govern their biosynthesis are largely unknown.

Afferent fibers play a central role in neurogenic inflammation. Neuropeptides, including calcitonin gene-related protein (CGRP)

and substance P, are released from afferent fibers (Saria, 1984; Brain and Williams, 1989). While both are potent vasodilators, their mechanisms of action differ. While CGRP promotes vasodilation, substance P increases capillary permeability. The impact of communication between nociceptors and non-neuronal cell types on injury repair is profound. Nociceptive mediators stimulate recruitment of immune cells and contribute to both innate and adaptive immunity (Pinho-Ribeiro et al., 2017). Regulated protein synthesis is critical in sensory neurons. Translational inhibition has been shown to reduce pain associated with inflammation, injury, neuropathy, and migraine (Ferrari et al., 2013a,b, 2015; Moy et al., 2017; Avona et al., 2019; Barragán-Iglesias et al., 2019; Megat et al., 2019). It is unclear which transcripts are subject to activity-dependent translation in afferent fibers. In the central nervous system, neuronal activity induces the expression of a number of effectors collectively referred to as immediate early genes (IEGs; Link et al., 1995; Lyford et al., 1995; Rosen et al., 1998; Guzowski et al., 1999; Vann et al., 2000).

To understand the impact of inflammatory mediators on the landscape of nascent translation in afferent neurons, we used ribosome profiling to analyze cultured dorsal root ganglion (DRG) neurons (Ingolia, 2010). Application of the inflammatory mediators nerve growth factor (NGF) and interleukin 6 (IL-6) induces persistent changes in the activity of DRG neurons (De Jongh et al., 2003; Svensson, 2010; Chang et al., 2016; Obreja et al., 2018). Based on altered patterns of ribosome occupancy, we identify numerous mRNAs with altered rates of translation. Intriguingly, we found a robust increase in biosynthesis of the prototypical IEG, Arc. Arc is critical for long-term forms of synaptic plasticity and memory (Plath et al., 2006; Shepherd and Bear, 2011). Moreover, dendritic translation of Arc mRNA is tightly correlated with activation of circuits implicated in learning and memory (McIntyre et al., 2005). A surprising connection has recently been established between Arc and retroviruses (Pastuzyn et al., 2018; Erlendsson et al., 2020). Arc protein is homologous to the HIV Gag protein and forms virus-like capsids. Arc mediates intercellular mRNA transport between neurons and a range of recipient cell types through extracellular vesicles (EVs). In *Drosophila*, the Arc homolog dArc1 transits from presynaptic neuromuscular synapses to muscle (Ashley et al., 2018). However, a precise physiologic function for intercellular communication mediated by Arc capsids remains to be determined in mammals. Here, we show that inflammatory signals promote rapid translation of Arc *in vivo* and *in vitro*. Mice that lack Arc have exaggerated thermal responses and vasodilation following an inflammatory challenge in the skin. Both are rescued by injection of Arc-containing EVs. Our data suggest a new role for Arc as a mediator of peripheral neuroinflammation.

Materials and Methods

Experimental model and subject details
In vitro experiments were performed using wild-type male Swiss Webster and C57BL/6J mice (four weeks old) purchased from Taconic Laboratories. Behavioral experiments were performed using male Swiss Webster, C57BL/6J and Arc^CreER mice (The Jackson Laboratory stock #021881) between the ages of 8 and 12 weeks, weighing ∼25–30 g at the start of the experiment. Animals were housed with a 12/12 h light/dark cycle and had food and water available *ad libitum*. All animal procedures were approved by Institutional Animal Care and Use Committee at The University of Texas at Dallas and were in accordance with International Association for the Study of Pain guidelines.

Ribosome profiling cultures
DRGs from cervical (C1) to lumbar (L5) spinal segment were excised from 10 mice per replicate and placed in chilled HBSS (Invitrogen). Following dissection, DRGs were enzymatically dissociated with collagenase A (1 mg/ml, Roche) for 25 min and collagenase D (1 mg/ml, Roche) with papain (30 U/ml, Roche) for 20 min at 37°C. DRGs were then triturated in a 1:1 mixture of 1 mg/ml trypsin inhibitor (Roche) and bovine serum albumin (BioPharm Laboratories), then filtered through a 70 μm cell strainer (Corning). Cells were pelleted, then resuspended in DRG culture media: DMEM/F12 with GlutaMAX (Thermo Fisher Scientific) containing 10% fetal bovine serum (FBS; Thermo Fisher Scientific), 1% penicillin and streptomycin, 5 ng/ml NGF, and 3 μg/ml 5-fluorouridine with 7 μg/ml uridine to inhibit mitosis of non-neuronal cells. The NGF added to the cultures is necessary to promote neuronal survival. Cells were evenly distributed in three poly-D-lysine-coated culture dishes (100 mm in diameter; BD Falcon) and incubated at 37°C in a humidified 95% air/5% CO₂ incubator. DRG culture media were changed every other day and cells were treated with NGF (20 ng/ml) and IL-6 (50 ng/ml) at day 6 for 20 min followed by addition of emetine (50 μg/ml) for 1 min to protect the ribosome footprints.

Library generation and sequencing
Libraries consisting of ribosome bound RNA fragments were generated as described with minor adjustments in the composition of the polysome lysis buffer [20 mM Tris-HCl, pH 7.5, 250 mM NaCl, 15 mM MgCl₂, 1 mM DTT, 0.5% (v/v) Triton X-100, 2.5 U/ml DNase I, 40 U/ml Rnasin, and 50 μg/ml emetine; Ingolia, 2010; Hornstein et al., 2016]. MicroSpin S-400 columns (GE Healthcare) were used to isolate ribosome bound RNAs. After rRNA was removed using RiboCop rRNA depletion kit (Lexogen), footprints were dephosphorylated then size selected (28–34 nucleotides) by PAGE on 15% TBE-Urea gels (Bio-Rad). Footprints were generated by SMARTer smRNA-Seq kit for Illumina (TaKaRa). RNA abundance was quantified using the Quantseq 3′ mRNA-Seq library kit (Lexogen). The concentrations of purified libraries were quantified using Qubit (Invitrogen) and the average size was determined by fragment analyzer with high sensitivity NGS fragment analysis kit (Advanced Analytical Technologies Inc.). Libraries were then sequenced on an Illumina NextSeq500 using 75-bp single-end high output reagents (Illumina).

After sequencing, files were downloaded from a BaseSpace onsite server. An Initial quality check was conducted using FastQC 0.11.5 (Babraham Bioinformatics). Adapters were subject to trimming based on adapter sequences. Mapping was conducted with TopHat 2.1.1 (with Bowtie 2.2.9) to the mouse reference genome (NCBI reference assembly GRCm38.p4) and reference transcriptome (Gencode vM10). Strand orientation was considered during the mapping process. Processed bam files were quantified for each gene using Cufflinks 2.2.1 with gencode. vM10 genome annotation. Read counts were not normalized by length by the using the Cufflinks option, no–length–correction. Relative abundance for the ith gene was determined by calculating transcripts per million (TPM) values as follows:

$$TPM_i = 10^6 \times \frac{a_i}{\sum_j a_j},$$ where a_j is the Cufflinks reported relative abundance.

Finally, TPM values were normalized to upper decile for each biological replicate and upper decile TPM (udTPM) were used for analysis (Glusman et al., 2013), to provide uniform processing for samples with varying sequencing depth. We also performed motif analysis using the Multiple Em for Motif Elicitation (MEME) Suite (Bailey et al., 2009).

Single-cell data
Single cell DRG sequencing data were generated based on published data (Li et al., 2016). Seurat package 2.2.1 (Butler et al., 2018) was used for visualization (Van der Maaten and Hinton, 2008).

Immunofluorescence, immunohistochemistry, and in situ hybridization
Spinal cord and L4–L5 DRG tissues were removed from adult 8- to 12-week-old mice and mounted using OCT mounting medium. Tissues were cryosectioned to 20-μm thickness and mounted onto Superfrost slides (Thermo Fisher Scientific). The sections were subsequently immersed in prechilled 10% formalin for 15 min and dehydrated in increasing concentration of ethanol (50%, 70%, and 100%). After complete drying, each section was carefully circled using a hydrophobic barrier pen (Immedge pen, RNAscope, ACDBio) and treated with Protease

IV (RNAscope Protease III and Protease IV Reagents kit, ACDBio) at 40°C for 2 min. The sections were then washed twice in PBS and target probes that can be detected in three different color channels, respectively (Atto 550, Alexa Fluor 488, and Atto 647) were added according to the manufacturer's protocol (RNAscope Fluorescent Multiplex Reagent kit). Briefly, the Arc (Arc, accession no. NM_018790.2, 20 bp, target region: 23–1066), CGRP (CGRP, accession no. NM_007587.2, 17 bp, target region: 44–995), and P2X3 probes (P2X3, accession no. NM_145526.2, 20 bp, target region: 795–1701) were added and incubated at 40°C for 2 h. Afterward, the sections were washed in RNAscope wash buffer twice and treated with the amplification reagent 1 (AMP1) for 30 min. There was a total of four amplification reagents (AMP1–AMP4) with alternating washes of 30- and 15-min incubation period. After the RNAscope protocol was completed, slides were blocked for 1 h in 10% normal goat serum (NGS), 0.3% Triton X-100 in 0.1 M PB. DRG slices were incubated overnight with a primary antibody against NF200 (1:500, Millipore, catalog #MAB5266). The next day, slides were incubated with goat anti-mouse Alexa Fluor 405 (1:1000, Thermo Fisher Scientific, A-31553) for 1 h. After additional PBS washes, slides were coverslipped with Prolong Gold antifade and allowed to cure for 24 h before imaging.

For immunohistochemistry, DRG, paw skin, and sciatic nerve sections were fixed in ice-cold 4% paraformaldehyde in 1× TBS for 1 h and then subsequently washed three times for 5 min each in 1× TBS. Slides were then incubated in a permeabilization solution made of 1× TBS with 0.4% Triton X-100 (Sigma-Aldrich) for 30 min and then were washed three times with 1× TBS. Tissues were blocked for at least 2 h in 10% heat-inactivated NGS in 1× TBS. Primary antibodies were used to detect the following proteins: GFP (1:1000, Aves labs, catalog #GFP-1020,), peripherin (1:1000, Novus, catalog #NBP1-05,423, NF200 (1:500, Millipore, catalog #MAB5266), CGRP (1:200, Enzo, catalog #BML-CA1134-0025), β-III tubulin (1:1000, Novus, catalog #NB100-1612). Primary antibodies were applied and incubated at 4°C overnight. The next day, slides were washed with 1× TBS and then appropriate secondary antibodies (Alexa Fluor, Invitrogen) were applied for 2 h. After additional washes, coverslips were mounted on slides with ProLong Gold antifade mountant (Invitrogen).

All of the images corresponding to immunohistochemistry and *in situ* hybridization samples were acquired using an FV-3000 confocal microscope (Olympus). For each DRG image, colocalization of *Arc/Calca* (CGRP) and *Arc/P2x3* (P2X3) was calculated using ImageJ plug-in JACoP (Bolte and Cordelières, 2006) and represented as % of Arc-positive cells expressing markers (*Calca* or *P2X3*). Colocalization (*Arc/NF200*) was assessed by counting the number of *Arc*-positive neurons that showed obvious *Arc* mRNA expression within the soma.

Protein immunoblotting

For *in vitro* experiments, Swiss Webster mice (four-week-old) were anesthetized with isoflurane and euthanized by decapitation. The DRGs from C1 to L5 spinal column were dissected and placed in chilled HBSS solution. Immediately after dissection, DRGs were dissociated and triturated as described above in the ribosome profiling culture protocol. After dissociation, cells from five mice were distributed evenly in a six-well plate coated with poly-D lysine and maintained at 37°C in a humidified 95% air/5% CO₂ incubator with fresh culture media replacement every other day. At day 6, the cells were treated with NGF (20 ng/ml) and IL-6 (50 ng/ml) for 20, 60, and 120 min. Cells were rinsed with chilled PBS, then lysed in lysis buffer (50 mM Tris, pH 7.4, 150 mM NaCl, 1 mM EDTA, pH 8.0, and 1% Triton X-100) containing protease and phosphatase inhibitors (Sigma-Aldrich). Total protein was extracted by ultrasonication and the supernatant was collected by centrifugation at 18,000 × *g* for 15 min at 4°C. Protein samples in 1× Laemmli sample buffer (Bio-Rad) were loaded and separated by 10% SDS-PAGE gels and then transferred to Immobilon-P membranes (Millipore). Membranes were blocked in Tris buffered saline (TBS) with 5% low-fat milk for 2 h at room temperature, then incubated overnight at 4°C with primary antibodies against Arc (1:300, Santa Cruz Biotechnology, catalog #sc-17 839), Alix (1:1000, Cell Signaling Technology, catalog #2171) or CD81(1:1000, Cell Signaling Technology, catalog #10037). After primary incubation, membranes were washed in TBST (TBS with 0.05% Tween

20) for 30 min (3 × 10 min) and incubated with secondary antibodies conjugated to horseradish peroxidase (Jackson ImmunoResearch) for 1 h at room temperature. The signal was detected using Western Chemiluminescent HRP Substrate (ECL; MilliporeSigma) on ChemiDoc Touch Imaging System (Bio-Rad). The blot was stripped in Restore Plus Western blot stripping buffer (Thermo Fisher Scientific) for 25 min and reincubated with primary antibody against GAPDH (1:10,000, Cell Signaling Technology, catalog #2118) or Actin (1:10,000, Cell Signaling Technology, catalog #4967) for 1 h at room temperature as an internal control. Membranes were washed 3 × 10 min in TBST and incubated with a secondary antibody for GAPDH or Actin. For the *in vivo* experiments, ipsilateral and contralateral paws, spinal cords and L4–L5 DRGs from adult 8- to 12-week-old C57BL/6J mice were rapidly removed and lysed in cell lysis buffer. Total protein was collected as described above. Analysis was performed using Image Lab 6.0.1 (Bio-Rad). Phosphorylated proteins were normalized to their respective total proteins and expressed as a percent of change compared with vehicle groups.

Sciatic nerve transection

Sciatic nerve axotomy is a well-accepted model in the pain field to study peripheral neuropathies. For these experiments, the left sciatic nerve of 8- to 12-week-old C57BL/6J mice was exposed and transected at mid-thigh level under isoflurane anesthesia. The wound was closed with 5–0 silk sutures. Following surgery, animals were housed and allowed to recover for 10 d before intraplantar NGF/IL-6 in the presence or absence of actinomycin D (Act D) administration. The additional procedure involving intraplantar NGF/IL-6 injection was approved by the UTD Institutional Animal Care and Use Committee (IACUC) on April 24, 2019.

Cloning

The PLJM1–eGFP vector (Addgene) was digested with NheI (Thermo Fisher Scientific) and EcoRI (Thermo Fisher Scientific) to excise the eGFP sequence. Mouse Arc CDS (Ensembl: ENSMUST00000023268.13) was cloned using the primers 5′-ATAAGCAGAGCTGGTTTAGTG AACCGTCAGATCCGCTAGCGCCACCATGGAGCTGGACCATAT-GACC-3′ and 5′-TGTGGATGAATACTGCCATTTGTCTCGAGGT CGAGAATTCCTATTCAGGCTGGGTCCTG-3′ from mouse brain cDNA into PLJM1 using Gibson assembly (Gibson et al., 2009).

F11 transfection

F11 cells were grown in DMEM/F-12 media (Thermo Fisher Scientific) supplemented with 10% FBS and 1% penicillin and streptomycin at 37°C at 5% CO₂. Cells were transfected with the Arc overexpression vector at a confluency of 70% using lipofectamine 3000 (Thermo Fisher Scientific). Transfection media were replaced with DMEM/F12 supplemented with 10% exosome free FBS and 1% penicillin and streptomycin after 6 h. Cells were washed twice with 1× PBS before media replacement. After 24 h, media from transfected cell lines was harvested for EV isolation and downstream assays.

EV isolation

EVs from F11 cells were isolated using total exosome isolation reagent (Thermo Fisher Scientific). Harvest media (7 ml) was spun down at 2000 × *g* for 30 min to remove cell debris. The supernatant was mixed with the isolation reagent in a ratio of (2:1) and incubated at 4°C for 16 h. After incubation, samples were centrifuged at 10,000 × *g* for 1 h to obtain a crude EV pellet. The pellet was resuspended in cold 1× PBS and centrifuged at 100,000 × *g* for 70 min to wash out contaminants. The final pellet was resuspended in cold 1× PBS and used for downstream applications. The final EV concentration was 300 ng/μl.

Vesicle exchange assay

Twenty-four hours after transfection, 7 ml of media were aspirated from donor cultures and centrifuged 2000 × *g* for 10 min. Media were aspirated again and centrifuged at 3000 × *g* for 20 min to remove cell debris. Media were removed from recipient cells, and the donor culture supernatant was transferred onto recipient cells and incubated for 24 h at 37° C and 5%CO₂. Cultures treated with dynamin inhibitors were incubated

with 80 μM Dynasore concurrently with media transfer. After 24 h, the cells were washed with 1× PBS and then lysed with 1× passive lysis buffer (Promega) for 10 min at 4°C. Firefly luciferase activity was assessed using LARII substrate (Promega); 100 μl of cell lysate was mixed with 50 μl of substrate, and luminescence was measured using a luminometer with an integration time of 10 s.

qPCR analysis
As a spike-in, 10 ng/100uL of firefly luciferase mRNA was added to isolated EVs before RNA extraction. RNA was purified from isolated EVs using TRIzol–LS (Thermo Fisher Scientific) following manufacturer's guidelines. cDNA synthesis was conducted using random hexamers and Improm-II reverse transcriptase (Promega). The resulting cDNA was used for qPCR via iQ SYBR Green Supermix (Bio-Rad). The primers used for qPCR are as follows: Arc, AAGTGCCGAGCTGAGATGC and CGACC TGTGCAACCCTTTC; firefly luciferase, TTCGACCGGGACAAAACCAT and ATCTGGTTGCCGAAGATGGG. qPCR was done on CFX96 Touch Real-Time PCR Detection System (Bio-Rad).

Cryo-EM specimen preparation, data collection, and analysis
EVs were flash frozen and stored at −80°C until use. Before preparing cryo-EM grids, the sample was diluted to 1.5 mg/ml as determined by a Bradford assay. C-flat grids (Copper, 1.2/1.3, Protochips) were prepared by glow-discharged for 30 s in a PELCO Easiglow glow-discharge unit at 15 mA. We applied 3 μl of EV in PBS to the grid and incubated for 60 s before vitrification using a FEI Vitrobot Mark IV (Thermo Fisher). The grids were blotted for 3 s using blotting force 3 at 4°C and ~90% humidity and plunged in liquid ethane.

Images were collected using a 626 Gatan cryo-holder on a TF20 microscope (FEI) equipped with a K2 Summit (Gatan) direct detector. We automated the collection of data using SerialEM (Mastronarde, 2005). A total of 60 movies 50 frames/movie) of each sample were acquired over 6.8 s with an exposure rate of 14.0 e⁻/pix/s, yielding a total dose of 56 e⁻/Å^2, and a nominal defocus range from −1.0 μm to −3.0 μm. Images were gain corrected using the method described by (Afanasyev et al., 2015) and motion-corrected in cisTEM (Grant et al., 2018). We measured the length and width of EVs in 20 consecutively collected images per sample manually in tdisp (https://sourceforge.net/projects/tigris/) and calculated mean and SD of counted vesicles per image.

Forward looking infrared (FLIR) imaging
Thermal changes in the hindpaw of vehicle-injected or complete Freund's adjuvant (CFA)-injected were visualized using a FLIR T31030sc thermal imaging camera (FLIR instruments). Animals were placed in acrylic boxes with wire mesh floors and imaged 24 h after CFA injection. Image analysis and quantification were performed using the FLIR ResearchIR Max four software available at http://support.flir.com/rir4.

Ultrasound imaging
Power Doppler ultrasound images of the hindpaw were acquired using a high-frequency ultrasound system (Vevo 3100, FUJIFILM VisualSonics Inc) equipped with an MX550D linear array transducer operating at 32 MHz. Data were collected from different planes by precise movement of the transducer along the elevational direction (step size = 38 μm) using a specialized 3D motorized stage. Data were processed using the Vevo software module (FUJIFILM VisualSonics) to calculate paw volume and percent vascularity.

Statistical analysis
In vitro data were collected from three independent cell cultures and are shown as mean ± SEM. All behavioral experiments were performed by blinded observers. Behavioral data are shown as mean ± SEM of at least six animals per group. For behavior experiments, sample size was estimated as $n = 6$ using G*power for a power calculation with 80% power, expectations of 50% effect size, with α set to 0.05. Graph plotting and statistical analysis used GraphPad Prism version 7.0 (GraphPad Software). Student's t test was used to compare two independent groups. Statistical evaluation for three independent groups or more was performed by one-way or two-way ANOVA, followed by post hoc Bonferroni, Dunnett, or Tukey test, and the a priori level of significance at 95% confidence level was considered at $p < 0.05$. Specific statistical tests used are described in figure legends. The significance of gene expression level changes before and after the treatment was calculated using a two-tailed Student's t test assuming unequal variances.

Results

Ribosome profiling identifies arc as a target of induced translation
To profile translation in the DRG, tissues were harvested from cervical (C1) to lumbar (L5) segments of the spinal column and maintained for 5 d in vitro (Fig. 1A). Cultures were subjected to either a vehicle treatment or exposed to two inflammatory mediators: NGF (20 ng/ml) and IL-6 (50 ng/ml). These molecules were selected because both rapidly induce nascent protein synthesis and lead to persistent changes in the activity of sensory neurons (Melemedjian et al., 2010). After 20 min, the elongation inhibitor emetine was added to each culture to stop translation and cells were lysed (Table 1). These samples were used to generate libraries for two types of sequencing. As a control for changes in mRNA abundance that could reflect transcription responses or changes in stability, mRNA levels were quantified with high-throughput sequencing. To generate these libraries, ribosome RNAs were depleted and 3′ end sequencing was conducted using Quantseq (Moll et al., 2014). The majority of the sample was used to generate the other type of library consisting of ribosome protected footprints. After translation was arrested with emetine, lysates were nuclease treated, small RNAs were purified, and adapters were added in a ligation independent manner (Hornstein et al., 2016). This process was repeated for a total of five independent replicates. The high-throughput sequencing experiments were highly reproducible both for ribosome profiling and for RNA-seq (Pearson's $R > 0.98$; Fig. 1B,C). We found that the majority of ribosome protected fragments mapped to annotated coding regions (Fig. 1D). To determine whether the treatment induced larger changes in mRNA abundance or translation, we compared differences in each dataset. We found that translation of 217 mRNAs was increased by >1.5-fold (Fig. 1E; Extended Data Fig. 1-1). To determine whether the preferentially translated mRNAs encoded products with related functions, we performed an ontological analysis. We found enrichment for several processes including: spinal cord injury (Fig. 1F, $p = 0.002$), IL-6 signaling ($p = 0.009$), and serotonin and anxiety-related events ($p = 0.0003$; Kuleshov et al., 2016).

Among the transcripts with significant increases in translation was the IEG Arc (Fig. 1G). While Arc is expressed in the spinal cord, it is unclear whether it is present in DRG neurons (Plath et al., 2006; Hossaini et al., 2010; Bojovic et al., 2015; Minatohara et al., 2015). To validate whether Arc is translated in response to inflammatory mediators, we conducted immunoblots on cultured DRG exposed to NG/IL-6 (Fig. 1H). We found little to no detectable Arc protein before addition of NGF and IL-6. However, 1 h after addition, Arc protein levels were increased by >15-fold. These results suggest that Arc is translated in response to inflammatory mediators in vitro.

We compared the treatment groups in depth using computational approaches. In both groups, the footprints displayed a triplet periodicity consistent with ribosomal translocation (Fig. 2A). While many transcripts displayed an increase in translation, fewer than 100 mRNAs displayed significant changes in abundance (Fig. 2B; Extended Data Fig. 1-2). Therefore, we focused our analysis on shared characteristics among targets of
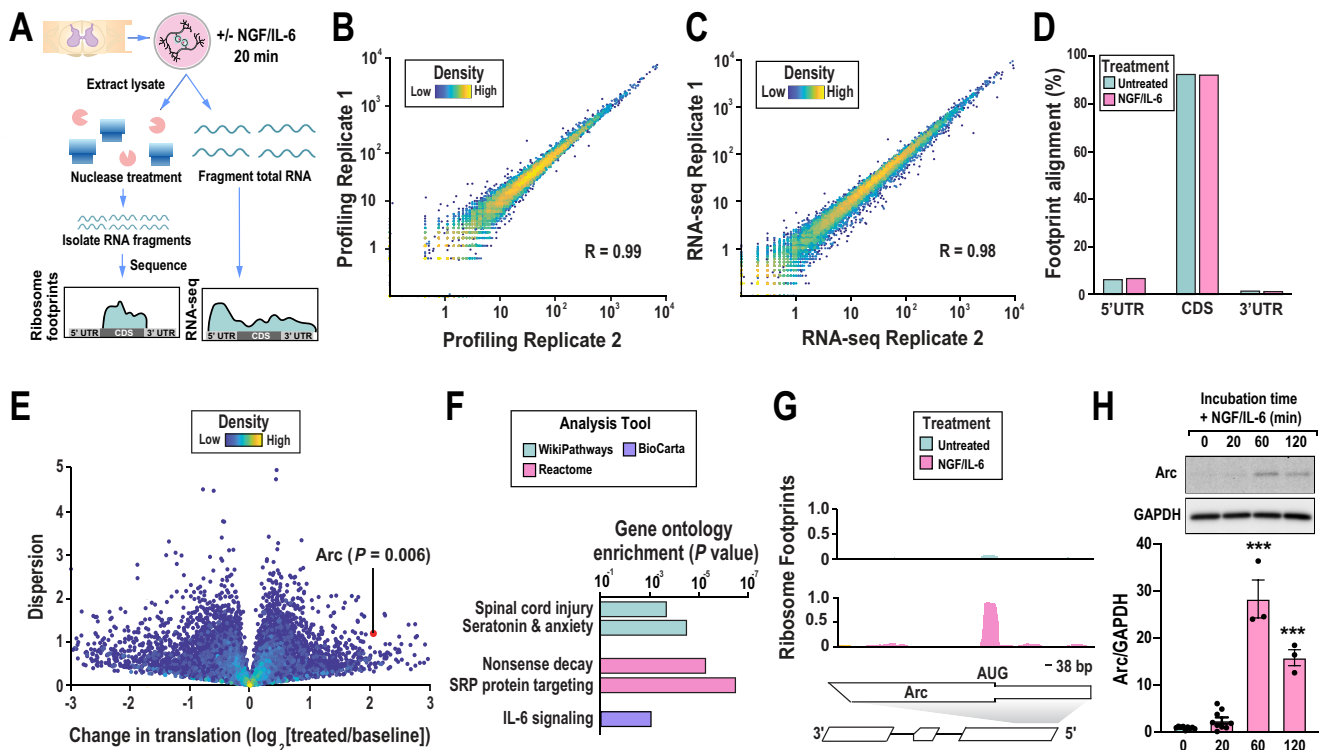
Figure 1. Ribosome profiling identifies Arc as a rapidly-translated gene. ***A***, Schematic representation of the ribosome profiling approach applied to DRG neurons. ***B***, Intraexperimental correlations for ribosome profiling in the inflammatory mediator treatment group. A list of genes with significant differences is translation is provided in Extended Data Figure 1-1. ***C***, Intraexperimental correlations for RNA-Seq in the inflammatory mediator treatment group. R values correspond to Pearson's correlations in ***B***, ***C***. Transcripts with significant changes in abundance are indicated in Extended Data Figure 1-2. ***D***, Aggregate sites of ribosome protected footprints in 5′ UTRs, coding sequences, and 3′ UTRs. ***E***, A volcano plot depicting changes in translation (log2 $\geq$ −1.5; false discovery rate < 0.05) across the transcriptome. The ratio of ribosome density following treatment with the inflammatory mediators divided by the vehicle levels is plotted against sample dispersion. Gene density is shaded according to the inset bar; p values for Arc were determined using a two-tailed Student's t test. ***F***, Gene ontology analysis of genes with significant translational enhancement was conducted with Enrichr (Kuleshov et al., 2016). ***G***, Traces of the 5′ end of Arc. Scales are indicated with bars. ***H***, Application of NGF/IL-6 to primary culture DRG neurons upregulated Arc protein in a time course of 0–120 min; $n = 9$ for 0- and 20 min groups, $n = 3$ for 60- and 120 min groups. Ordinary one-way ANOVA: $F_{(3,20)} = 95.79$, $p < 0.0001$. Dunnett's multiple comparisons test: 0 versus 20 min, ***$p < 0.001$; 0 versus 120 min, ***$p < 0.001$.

differential translation. To determine what features were commonly observed in this set of transcripts we examined 5′ untranslated region (UTR) length and GC content (Fig. 2C,D). While we did not detect an overt difference, we found a nine-base motif that was significantly enriched in the 5′ UTR (Fisher's exact test, $p = 0.02$; Fig. 2E,F). This sequence motif is highly reminiscent of an mTOR responsive element termed the pyrimidine-rich translational element (Hsieh et al., 2012). Based on the collective analyses, we conclude that cultured DRG neurons preferentially translate genes linked to neuronal function in response to brief exposure to inflammatory mediators and memory and are enriched for a specific motif found in the 5′ UTR.

Arc mRNA is expressed mainly in large diameter DRG neurons

Next, we sought to determine whether *Arc* mRNA is preferentially expressed in a specific class of sensory neuron *in vivo*. To identify cells that express *Arc*, we analyzed single cell sequencing previously conducted on dissociated DRG neurons (Li et al., 2016; Fig. 3A). We qualitatively compared expression of *Arc* to markers for peptidergic (*Calca/CGRP*), non-peptidergic (*P2X3*), and a light chain neurofilament expressed in large diameter neurons (*NELF*). *Arc* is expressed at low levels in a range of cell types but lacks a clear bias in the single cell sequencing experiments. To examine the expression of *Arc* in tissues, we conducted *in situ* hybridization on L4–L5 DRG tissues harvested from animals exposed to the inflammatory mediators (henceforth referred to

as ipsilateral) or negative controls collected from the same animals on the uninjected side of the body (henceforth contralateral; Fig. 3B). Using the same series of markers, we find instances where *Arc* expression coincides with each marker. However, *Arc* levels are highest in large diameter neurons that express NF200 and peptidergic neurons that express *Calca* (Fig. 3C). *Arc* expression was found to be increased by strong nociceptive stimuli in the spinal cord (Hossaini et al., 2010). However, we found no clear differences in *Arc* expression in the DRG or spinal cord (Fig. 3D,E) following injection of NGF/IL-6. As a control for the specificity of our *in situ* hybridization probes, we repeated our experiments with a negative control RNA probe for *Arc* and found little to no detectable signal in either the DRG or spinal dorsal horn (Extended Data Fig. 3-1A–C).

To test whether Arc is expressed in DRG neurons *in vivo*, we made use of an EGFP-Arc reporter strain. In these mice, Arc is expressed as a translational fusion to EGFP downstream of a full-length Arc promoter (Okuno et al., 2012; Steward et al., 2017). An ideal property of this model is that *Arc* is translated at higher levels than the endogenous transcript under baseline conditions. This is partially because of escape of the reporter from non-sense-mediated decay as an intron in the endogenous *Arc* 3′ UTR is absent in the transgene. We performed immunohistochemistry on DRG tissues using broad neuronal marker, peripherin, and examined its co-localization with EGFP-Arc (Fig. 4A). We found that Arc is expressed in DRG neurons. Next, we examined expression of EGFP-Arc in large diameter neurons and

Table 1. List of animals, antibodies, chemicals, reagents, commercial assays, recombinant proteins, peptides, and software and algorithms used in this study

Reagent or resource	Source	Identifier
Antibodies		
Rabbit monoclonal anti-GAPDH(14C10)	Cell Signaling Technology	Catalog #2118
Mouse monoclonal anti-Arc (C-7)	Santa Cruz Biotechnology	Catalog #sc-17839
Goat anti-mouse IgG, Alexa Fluor 405	Thermo Fisher Scientific	Catalog #A31553
Mouse monoclonal anti-Neurofilament 200 kDa (N52)	MilliporeSigma	Catalog #MAB5266
Goat anti-mouse IgG, light chain specific	Jackson ImmunoResearch	Catalog #115-035-174
Goat anti-rabbit IgG (H + L)	Jackson ImmunoResearch	Catalog #111-036-144
Mouse monoclonal anti-Alix (3A9)	Cell Signaling Technology	Catalog #2171
Rabbit monoclonal anti-CD81 (D5O2Q)	Cell Signaling Technology	Catalog #10037
Rabbit polyclonal anti-β-actin	Cell Signaling Technology	Catalog #4967
Rabbit monoclonal anti-GFP	Cell Signaling Technology	Catalog #2956
Chicken polyclonal anti-peripherin	Novus Biologicals	Catalog #NBP1-05423
Chemicals, peptides, and recombinant proteins		
DMEM/F-12, GlutaMAX supplement	Gibco	Catalog #10565018
HBSS	Gibco	Catalog #14170112
Collagenase A	Roche	Catalog #10103578001
Collagenase D	Roche	Catalog #11088858001
Papain	Roche	Catalog #10108014001
Trypsin inhibitor	Roche	Catalog #10109886001
Bovine serum albumin	Thermo Fisher Scientific	Catalog #BP1600-100
FBS, premium select	R&D Systems	Catalog #S11550
5-Fluoro-2′-deoxyuridine	Sigma-Aldrich	Catalog #F0503
Uridine	Sigma-Aldrich	Catalog #U3003
Poly-D-lysine hydrobromide	Sigma-Aldrich	Catalog #P7886
Mouse NGF 2.5S protein	MilliporeSigma	Catalog #01-125
Recombinant mouse IL-6 protein	R&D Systems	Catalog #406-ML-005
Emetine, dihydrochloride	MilliporeSigma	Catalog #324693
RNase-free DNase I	Lucigen Corporation	Catalog #D9905K
RNasin ribonuclease inhibitors	Promega Corporation	Catalog #N2111
Prostaglandin E2	Cayman Chemical	Catalog #14010
NGS	Sigma-Aldrich	Catalog #NS02L
DAPI	Thermo Fisher Scientific	Catalog #D1306
ProLong Gold antifade mountant	Thermo Fisher Scientific	Catalog #P36930
Protease inhibitor cocktail powder	Sigma-Aldrich	Catalog #P2714
Phosphatase inhibitors cocktail 2 and cocktail 3	Sigma-Aldrich	Catalog #P5726 and P0044
Total exosome isolation reagent	Thermo Fisher Scientific	Catalog #4478359
Lipofectamine 3000 transfection reagent	Thermo Fisher Scientific	Catalog #L3000008
Promega ImProm-II reverse transcription	Thermo Fisher Scientific	Catalog #PRA3800
iQ SYBR Green Supermix	Bio-Rad Laboratories	Catalog #1708886
Critical commercial assays		
Western chemiluminescent HRP substrate (ECL)	MilliporeSigma	Catalog #WBKLS0500
SMARTer smRNA-Seq kit for Illumina	Takara Bio USA, Inc	Catalog #635031
QuantSeq 3′ mRNA-Seq library prep kit FWD for Illumina	Lexogen	Catalog #015.96
RiboCop rRNA depletion kit V1.2	Lexogen	Catalog #037.96
Qubit dsDNA HS assay kit	Thermo Fisher Scientific	Catalog #Q32851
High-sensitivity NGS fragment analysis kit	Advanced Analytical Technologies, Inc	Catalog #DNF-474
NextSeq 500/550 high-output v2 kit (75 cycles)	Illumina	Catalog #FC-404-2005
RNAscope Protease III and Protease IV reagents kit	Advanced Cell Diagnostics	Catalog #322340
RNAscope multiplex fluorescent detection kit	Advanced Cell Diagnostics	Catalog #320851
RNAscope wash buffer reagents	Advanced Cell Diagnostics	Catalog #310091
RNAscope Probe, Mm-Arc	Advanced Cell Diagnostics	Catalog #316911
RNAscope Probe, Mm-Calca-alltv-C2	Advanced Cell Diagnostics	Catalog #417961-C2
RNAscope Probe, Mm-P2rx3-C3	Advanced Cell Diagnostics	Catalog #521611-C3
Deposited data		
Sequencing deposited to GEO	https://www.ncbi.nlm.nih.gov/geo/query/acc.cgi?acc=GSE117043	GSE117043 (token for access: efgpqousplafvif)
Experimental models: organisms/strains		
Swiss Webster Mice	Taconic Laboratories	Model #SW-M
C57BL/6J Mice	Taconic Laboratories	Model #B6-M
B6.129(Cg)-Arc$^{tm1.1(cre/ERT2)Luo}$/J Mice	The Jackson Laboratory	Catalog #021881
C57BL/6-Tg(Arc-EGFP/Arc)3Hbto	RIKEN BioResource left	RBRC06086
Oligonucleotides		
Primers	Sigma	
Recombinant DNA		
PLJM1, Arc	This manuscript	

(Table continues.)

Table 1. Continued

Reagent or resource	Source	Identifier
PGL4.13[luc2/SV40]	Promega	Catalog #E6681
Software and algorithms		
TopHat 2.1.1	https://ccb.jhu.edu/software/tophat/index.shtml	
Bowtie 2.2.9	http://bowtie-bio.sourceforge.net/bowtie2/index.shtml	
Cufflinks 2.2.1	http://cole-trapnell-lab.github.io/cufflinks/	
SerialEM	https://bio3d.colorado.edu/SerialEM/	Mastronarde (2005)
cisTEM	https://cistem.org/	Grant et al. (2018)
Tdisp	https://sourceforge.net/projects/tigris/	

found evidence of co-localization both in the DRG and in the sciatic nerve (Fig. 4B,C). The reporter strain suggests that Arc is present throughout the DRG and is particularly abundant in large diameter neurons that express NF200. Finally, we asked whether Arc was expressed in fibers that innervate the skin. We observed co-localization with CGRP and the neuronal marker β-III tubulin (Fig. 4D,E).

Local translation of arc in the paw

To determine whether inflammatory mediators induce rapid translation of endogenous Arc *in vivo*, we examined Arc levels in skin from the hindpaw of injected or uninjected paws 1 h after treatment. Immunoblots show that the treatment induces rapid translation of Arc in the ipsilateral paw (Fig. 5A). To test whether Arc production is the result of *de novo* transcription or translation of preexisting mRNA, a transcription inhibitor (Act D) was included in the treatment (Fig. 5A). Inhibition of transcription did not significantly diminish induced translation of Arc, suggesting that Arc is likely translated from the population of existing mRNA. Next, we asked whether Arc translation is induced in either the DRG or the dorsal horn of the spinal cord. In both tissues, Arc is detected, but levels are not increased by NGF/IL-6 treatment (Fig. 5B,C).

Arc is expressed in skin-migratory dendritic cells, thus, we sought to identify the cell type responsible for Arc production in the skin (Ufer et al., 2016). To determine whether neurons are the relevant source, afferent fibers were eliminated through transection of the sciatic nerve on the ipsilateral side (Fig. 5D). Transection of the sciatic nerve causes a complete loss of afferent fibers in the ipsilateral paw (Devor and Wall, 1981; Tandrup et al., 2000). After animals were allowed to heal for a period of 10 d, NGF/IL-6 treatment was repeated. Arc expression was not increased as a result of the surgery. Injection of NGF/IL-6 on animals subjected to transection of the sciatic nerve no longer triggered an increase in Arc biosynthesis (Fig. 5E). Additionally, transection of the sciatic nerve did not change Arc abundance in the DRG (Fig. 5F). Taken together, our data support the conclusion that NGF/IL-6-induced translation of Arc in the skin is likely because of local translation in afferent fibers.

Arc-containing EVs can rescue inflammatory responses in the skin of Arc-deficient mice

Given that Arc forms virus-like capsids that mediate mRNA transfer between different cell types, we hypothesized that Arc could facilitate communication between neurons and non-neuronal cells in the skin via EVs. Overexpression of Arc in HEK293 cell lines yields Arc-containing EVs capable of mRNA transport (Pastuzyn et al., 2018). Arc is present in purified EVs, but the precise mechanism of its biogenesis is unclear. Given the viral origin of Arc, its biogenesis pathway may not parallel that of classic

EVs. To determine whether nociceptors are capable of generating functional Arc in EV preparations, we made use of a nociceptor cell line derived from rat DRG neurons designated as F11 (Platika et al., 1985). Arc was expressed in F11 cells using a recombinant vector. EVs were enriched from bulk media using an EV isolation reagent (Table 1). Afterward, dead cells were removed by low-speed centrifugation. Vesicles were concentrated by ultracentrifugation and subjected to a gentle wash before resuspension. We subjected EV fractions to cryo-EM, then counted and characterized the morphology of the observed spherical particles ranging in size from ∼20 to 200 nm (Fig. 6A,B). Transfection of the F11 nociceptor cell line with Arc lead to an ∼3.9-fold increase of EVs per image (3.5 ± 1.7 vesicles/image in the control vs 13.7 ± 4.1 vesicles/image for transfected; Fig. 6C). Visualization by cryo-EM of vesicles obtained from Arc-transfected cells revealed a higher abundance of vesicles smaller than 200 nm as compared with the untransfected control (Extended Data Fig. 6-1).

As an additional test for the presence of Arc purified EV samples, we measured Arc protein release in EVs using Western immunoblotting (Fig. 6D). Untransfected cells have little detectable endogenous Arc in either the cell pellet or in the EV fraction. In contrast, transfected cells show strong enrichment for Arc in the EV fraction. These EVs were highly enriched for known EV markers (e.g., ALIX, CD81, actin; Andreu and Yáñez-Mó, 2014; Willms et al., 2018). Arc-containing vesicles produced in HEK293 cells and cortical neurons show strong enrichment for the *Arc* mRNA (Pastuzyn et al., 2018). Using qPCR, we found that *Arc* mRNA can be robustly detected in EVs isolated from F11 cells expressing Arc (Fig. 6E). We conclude that forced Arc expression in F11 cells results in accumulation of Arc protein in EV preparations.

Arc vesicles mediate intercellular transfer of abundant mRNAs (Pastuzyn et al., 2018). As a functional test of Arc intercellular transfer obtained from purified EVs derived from nociceptors, we co-transfected Arc with a vector that encodes a firefly luciferase reporter (Fig. 6F). While the precise specificity of Arc for mRNA is not known, recombinant Arc binds non-specifically to RNA with high affinity (Pastuzyn et al., 2018). We reasoned that non-specific associations with highly abundant transcripts were possible on forced overexpression. Donor cells were transfected with Arc and the reporter, media were then replaced 6 h later to remove residual complexes between DNA and transfection reagent. One day later, the media were collected and centrifuged to remove cell debris. The clarified media were placed on a recipient F11 culture and allowed to incubate for 1 d. Afterward, media were removed, and lysates were subjected to luminescence assays. We found that transfected cultures yielded substantial luciferase activity (Fig. 6G). Transfer of the media from donor cells expressing luciferase reporter alone to non-transfected recipient cells resulted in little detectable activity (Fig. 6H). In contrast,
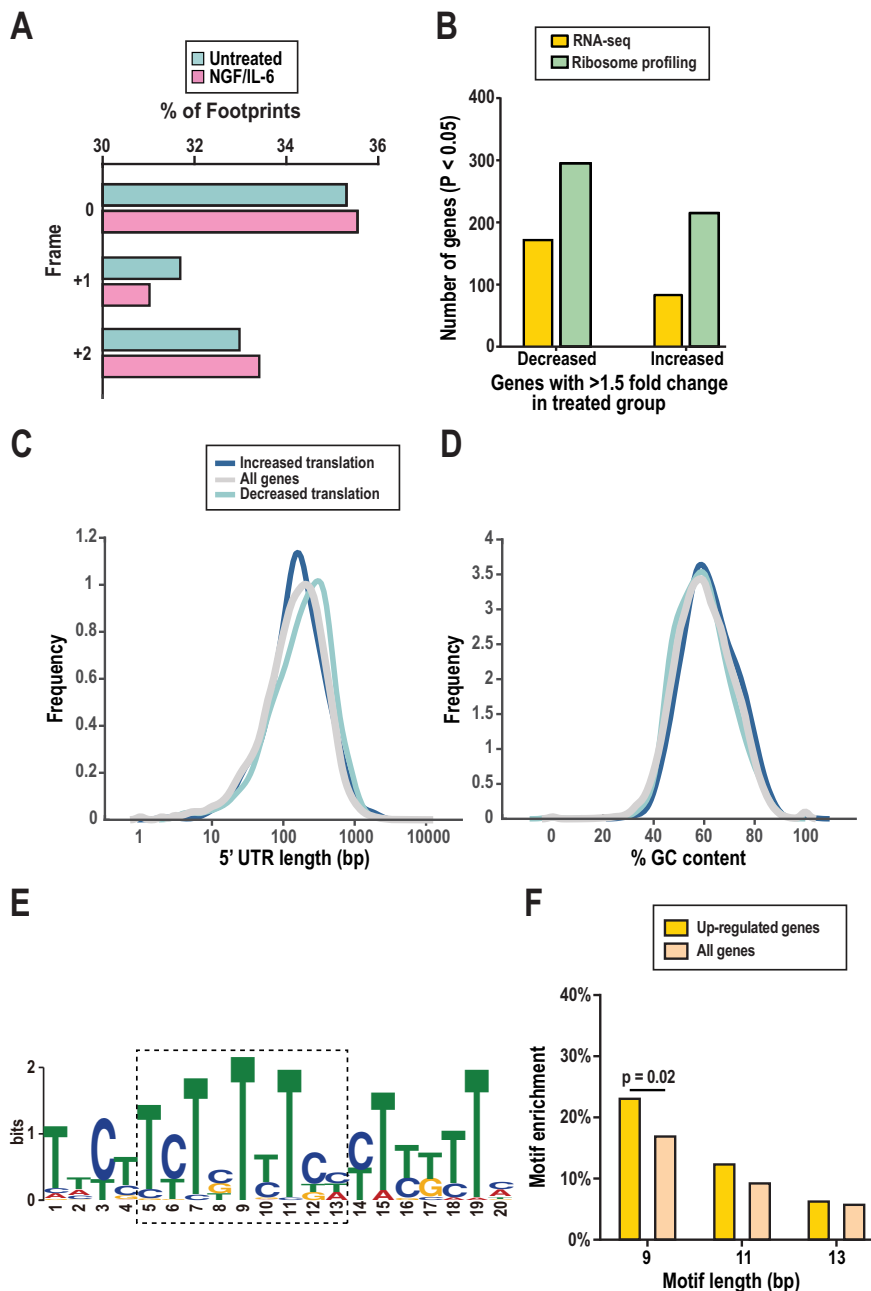
Figure 2. Bioinformatic analysis of differentially translated genes. *A*, Phase of ribosome protected footprints. *B*, To be considered a gene with a significant change in abundance or translation, a 1.5-fold (50% upregulated, or 33% downregulated) change and a significance value of <0.05 was required (Student's *t* test, two-tailed, assuming unequal variances between the two groups tested). *C*, Comparative analysis of UTR length. *D*, GC bias in 5′ UTRs. *E*, A pyrimidine-rich translational element (PRTE) was detected with MEME (*E* value 4.1×10^{-58}; 1). *F*, A core PRTE is significantly enriched in preferentially translated 5′ UTRs; *p* value estimate from Fisher's exact test.

response to noxious stimuli (Richardson and Vasko, 2002). Vasodilation increases blood flow to the skin which results in an increase in skin temperature (Chiu et al., 2012; Tanda, 2015). This increase in temperature can be detected by non-invasive FLIR thermal imaging. To determine whether Arc plays a role in neuroinflammation, we examined the temperature of the paw after a strong inflammatory challenge. We made use of a genetic model where a CreER reporter transgene induces polyadenylation before the Arc coding sequence (Guenthner et al., 2013). We found that homozygous animals have little remaining Arc in either the skin or the DRG (Extended Data Fig. 7-1). Because intraplantar injections of modest amounts of IL-6 and NGF do not elicit overt changes in the temperature of the paw, we made use of a more robust inflammatory mediator called CFA that increases levels of both NGF and IL-6 (Safieh-Garabedian et al., 1995; Su et al., 2012). Injection of CFA into the paw of mice results in a rapid increase in blood flow that manifested as an increase in temperature using FLIR (Fig. 7A). The average increase in paw temperature in wild-type animals was 1.4°C, across a 72-h period. In contrast, lack of Arc resulted in a much higher increase in paw temperature, averaging at 2.6°C. This effect was significant at 3 and 24 h after CFA administration (Fig. 7A,B). Collectively, these data suggest that Arc is required to attenuate increases in skin temperature triggered by inflammation.

To determine whether Arc-containing EVs are able to rescue inflammatory responses in Arc-deficient animals, we injected the ipsilateral paw with 1 µg of vesicles purified from either Arc-overexpressing or non-transfected F11 cells and examined paw temperatures using FLIR. Injection of Arc-containing EVs rescued excessive heat responses in Arc knock-out (KO) animals at 3, 24, and 48 h (Fig. 7C). In contrast, injection of EVs obtained from non-transfected cells did not diminish the increase in hind paw temperature. Collectively, these data suggest that Arc-containing EVs derived from nociceptor cells can restore normal functional responses in the skin of Arc KO mice

We wondered whether the cause of the increased thermal responses to CFA was driven by vasodilation. As a measure of blood flow, we made use of three-dimensional (3-D) high-frequency ultrasound imaging. In these assays, blood flow is measured using a power Doppler method. We found that following injection of CFA, relative blood flow in paws was higher in Arc-deficient animals relative to wild-type mice (Fig. 7D). However, the amount of swelling was not

transfer of media from cultures co-expressing Arc and luciferase resulted in an increase in light production of 445%. Transfer requires endocytosis in recipient cells as luciferase expression was diminished in cultures treated with a dynamin inhibitor (Dynasore). We conclude that Arc-containing EVs obtained from a nociceptor cell line are functionally similar to those obtained from HEK293 cells or primary hippocampal neurons in that they are capable of carrying mRNA cargos encoding other proteins (Pastuzyn et al., 2018).

Neurogenic inflammation plays a key role in vasodilation through release of neuropeptides from primary afferent fibers in
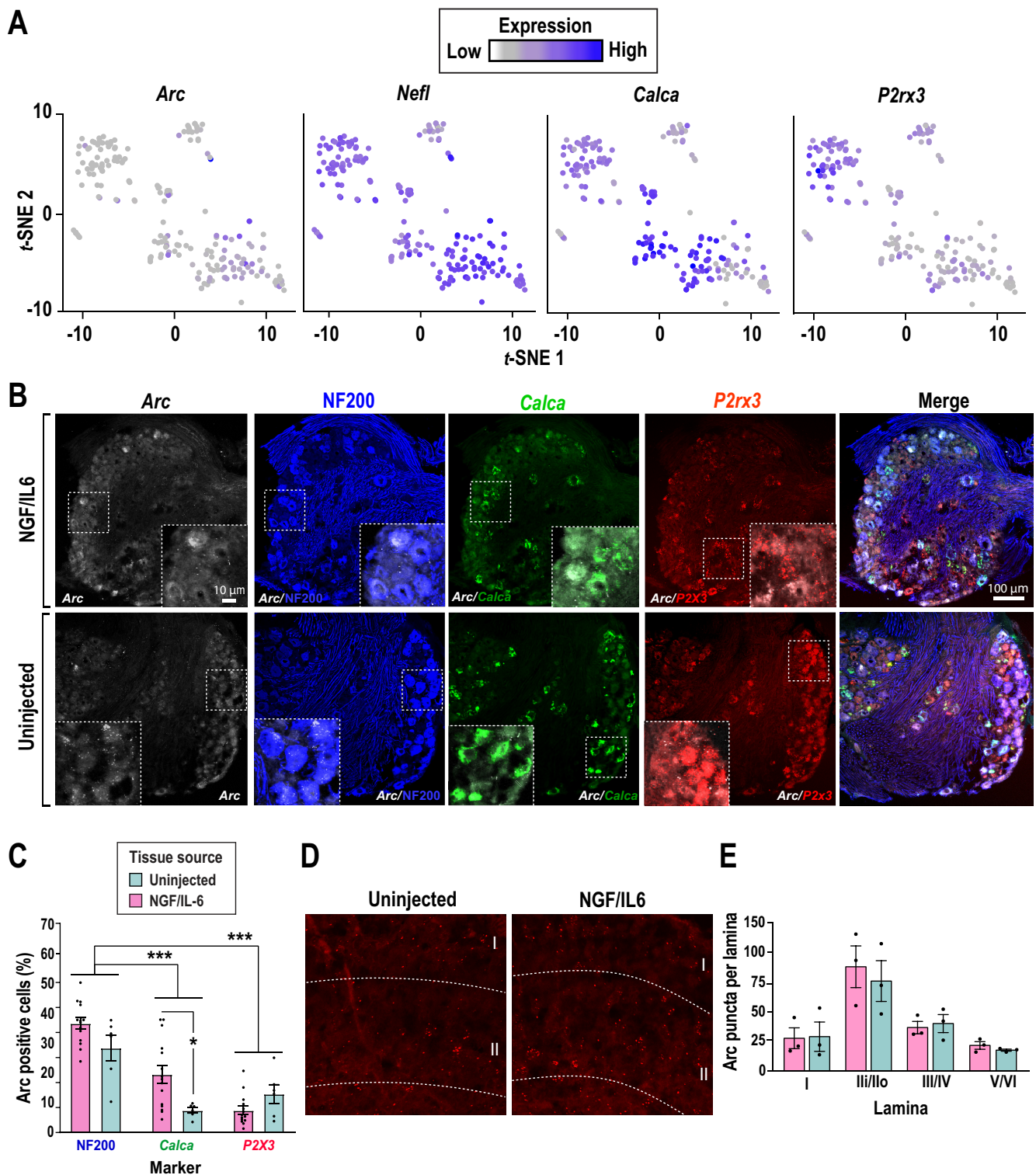
Figure 3. *Arc* is constitutively expressed in peripheral and spinal sites important for nociceptive signaling. ***A***, Single DRG neuron-sequencing tSNE clusters showing expression of *Arc* with the light neurofilament expressed in large diameter neurons (*Nefl*) and across DRG sensory neurons of peptidergic; *Calca* (CGRP) and non-peptidergic [*P2x3* (P2X3)] subclusters (Li et al., 2016). ***B***, *In situ* hybridizations of Arc and markers for L4–L5 DRGs together with large diameter neurons expressing neurofilament protein NF200 (NF200, blue), *Calca* (CGRP, green), and neurons expressing *P2x3* (P2X3 red). Validation for negative control probes is provided in Extended Data Figure 3-1. ***C***, Quantification of *Arc* expression in the DRG. Expression of *Arc* is greatest in NF200 expressing large diameter neurons. Intraplantar administration of the inflammatory mediators increased *Arc* mRNA in ipsilateral (IPL) DRGs expressing *Calca* (CGRP) mRNA; $n = 3$ animals per group; multiple slices from L4–L5 DRGs. Two-way ANOVA: cell-type factor, $F_{(2,55)} = 35.80$, $p < 0.0001$; treatment factor, $F_{(1,55)} = 4.545$, $p = 0.0375$. Bonferroni's multiple comparisons test: NF200 versus CGRP, ***$p < 0.0001$; NF200 versus P2XR, ***$p < 0.0001$; CGRP-IPL versus CGRP-CL, *$p = 0.0113$. ***D***, *In situ* hybridization of *Arc* in the dorsal horn of the spinal cord (Lamina I–VI). ***E***, Quantification of ***D***. *Arc* expression is highest in Laminal Layer II. Intraplantar administration of inflammatory mediators did not significantly impact *arc* mRNA expression.
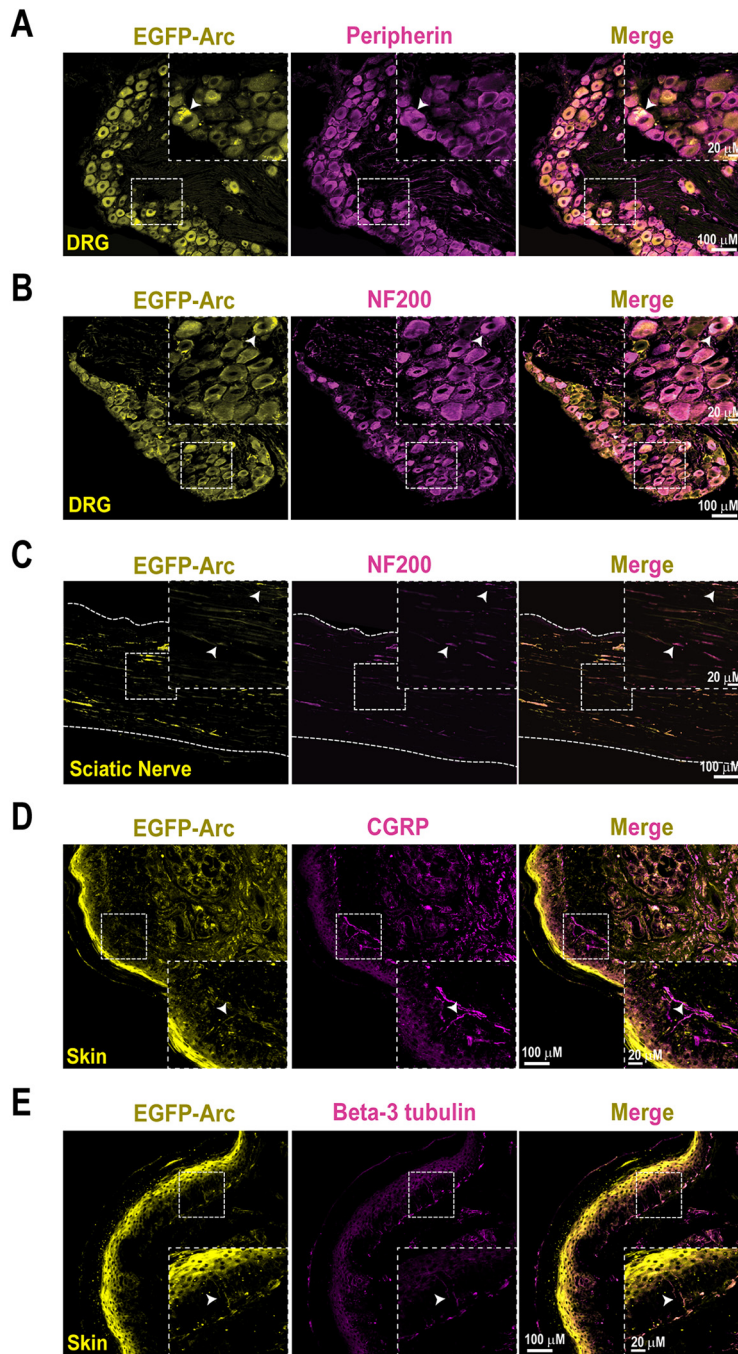
A, EGFP-Arc | Peripherin | Merge — DRG

B, EGFP-Arc | NF200 | Merge — DRG

C, EGFP-Arc | NF200 | Merge — Sciatic Nerve

D, EGFP-Arc | CGRP | Merge — Skin

E, EGFP-Arc | Beta-3 tubulin | Merge — Skin

Figure 4. Expression of eGFP-Arc. *A*, eGFP-Arc is ubiquitously expressed in the DRG and co-localizes with peripherin expressing neurons. *B*, eGFP-Arc is expressed in large diameter DRG neurons that express NF200 in the DRG. *C*, Expression patterns in the sciatic nerve for eGFP-Arc and NF200. *D*, eGFP-Arc is expressed in the glabrous skin and co-localizes with CGRP-expressing fibers. *E*, eGFP-Arc is expressed in the glabrous skin and co-localizes with β-III tubulin-expressing fibers. Arrowheads indicate colocalization.

Discussion

We describe a novel role for intercellular Arc signaling in nociceptor mediated neuroinflammatory responses in the skin. The unexpected finding that Arc mediates cell-to-cell communication similar to retrovirus "infection" has prompted speculation as to what kind of functional role this pathway may control (Kedrov et al., 2019). We posit that translation of Arc in DRGs in response to inflammatory signals, could lead to the generation and release of Arc-containing EVs that regulate inflammation in the skin. Furthermore, our observations have broad implications for the identification of targets of translational control in sensory neurons. The ability to precisely control treatments consisting of inflammatory mediators coupled to global measurement of nascent protein synthesis affords unique opportunities to identify targets of preferential translation. This work complements related efforts to profile translation in tissues (Uttam et al., 2018; Megat et al., 2019). We focused on identification of transcripts that display rapid changes in translation as opposed to regulatory changes that manifest days after an injury. Our reasoning was that widespread changes in transcription were likely to be minimal after only 20 min. Indeed, the number of transcripts with significant changes in translation is nearly double that of those whose levels change in abundance (Fig. 2B). We identified multiple IEGs (e.g., Egr2, Fos) that were preferentially translated in response to a brief treatment with inflammatory mediators. We focused specifically on Arc because it is rapidly transcribed in the brain and localized to dendrites before local translation and because of its recently established roles related to intercellular signaling (Link et al., 1995; Lyford et al., 1995; Steward et al., 1998; Ashley et al., 2018; Pastuzyn et al., 2018). Disruption of Arc through knock-down or genetic ablation results in profound deficits in learning and memory (Guzowski et al., 2000; Plath et al., 2006). Yet, Arc remains poorly characterized in sensory neurons. Our observations enable three major conclusions.

Our experiments uncover a new function for Arc in the periphery. We found that Arc plays a role in inflammation. Two of the best characterized nociceptive transmitters are CGRP and substance P (Saria, 1984; Brain and Williams, 1989). Both are potent vasodilators released from sensory fibers in response to noxious cues. Intriguingly, Arc appears to function in an opposing manner. In the skin, Arc is present in fibers that contain CGRP. An intriguing possibility is that Arc antagonizes CGRP release. But why would different subsets of sensory neurons produce signaling

significantly different between groups at 24 h (Fig. 7E). To determine whether Arc-containing EVs attenuate the increase in blood flow, we injected Arc-deficient animals with 1 µg of purified EVs (Fig. 7F). We found that the Arc-containing EVs rescued abnormal vasodilation whereas the negative control EVs did not normalize elevated blood flow. When taken together with the FLIR measurements, our data suggest that intercellular Arc signaling constrains neurogenic inflammation in the periphery.
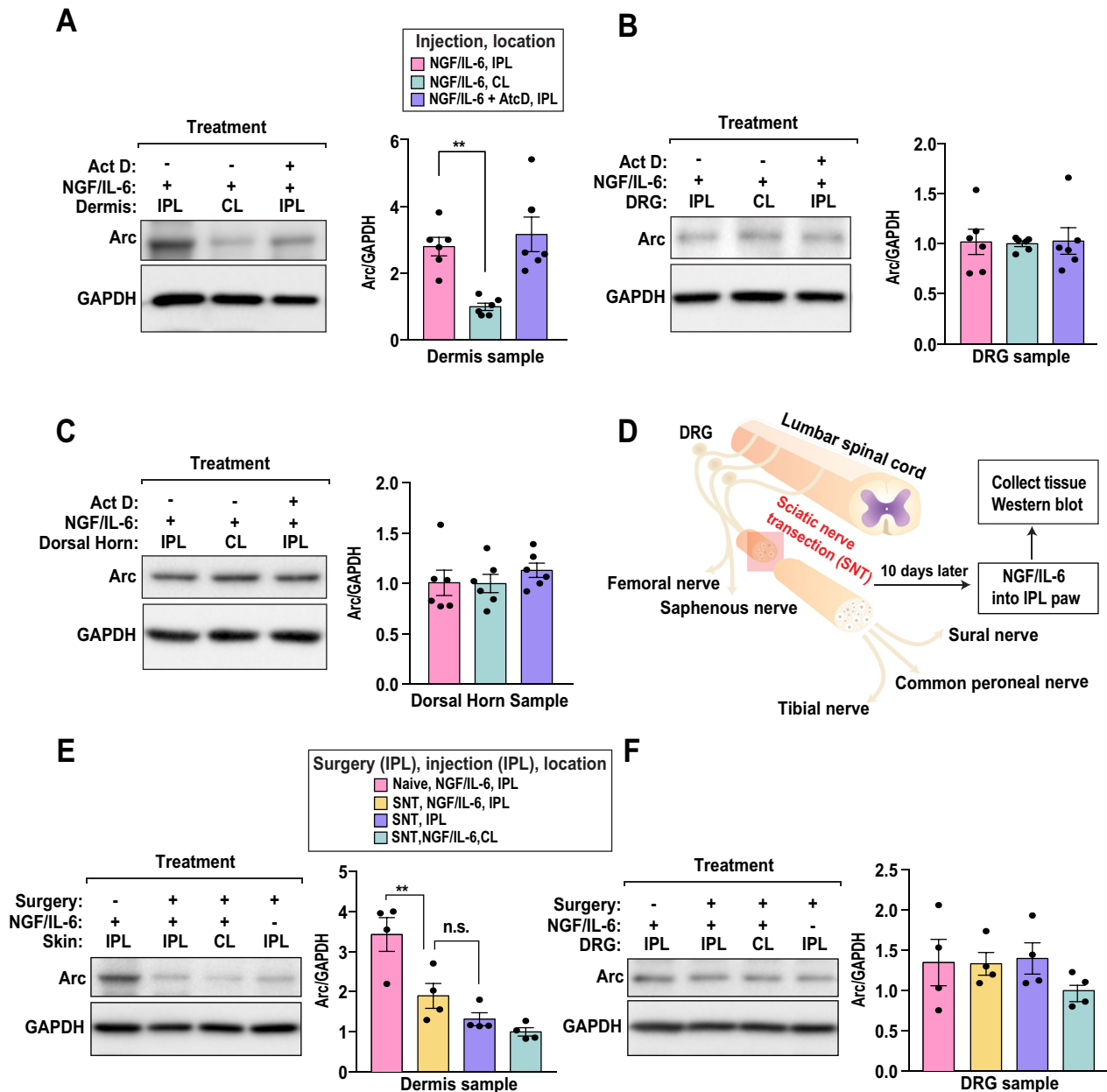
Figure 5. Induced biosynthesis of Arc in the skin depends on the presence of intact primary afferents. **A**, Intraplantar administration of inflammatory mediators in the ipsilateral (IPL) paw of mice triggered a rapid translation of arc in skin that is not modified by the transcription inhibitor Act D (300 ng/25 μl); $n = 6$ animals per group. Ordinary one-way ANOVA: $F_{(2,15)} = 11.33$, $p = 0.0010$. Bonferroni's multiple comparisons test: NGF/IL-6, IPL versus NGF/IL-6, CL; **$p = 0.0022$. IPL, ipsilateral or injected side; CL, contralateral or uninjected side. **B**, Intraplantar administration of inflammatory mediators, in the presence or absence of Act D (300 ng/25 μl), did not alter Arc abundance in the DRG. **C**, Intraplantar administration of inflammatory mediators, in the presence or absence of Act D (300 ng/25 μl), did not modify Arc abundance in the spinal dorsal horn (SDH). **D**, A cartoon detailing the experimental protocol for sciatic nerve transection (SNT). Sciatic nerve was axotomized, and 10 d later, animals received an intraplantar injection of the inflammatory mediators. One hour after injection, Arc protein expression was analyzed in DRG and glabrous skin from injected (ipsilateral, IPL) and noninjected (contralateral, CL) paws. **E**, Increase in Arc abundance in the skin caused by intraplantar administration of inflammatory mediators requires intact primary afferent fibers; $n = 4$ animals per group. Ordinary one-way ANOVA: $F_{(3,12)} = 15.14$, $p = 0.0002$. Tukey's multiple comparisons test: naive, NGF/IL-6, IPL versus SNT, NGF/IL-6, IPL; **$p = 0.0094$. n.s., non-significant. **F**, SNT surgery transection did not alter Arc abundance in the DRG.

molecules with opposing effects on the same process? Transcriptional control of the lipopolysaccharide (LPS) response in macrophage provides a relevant parallel. LPS induces rapid transcription of genes that encode functionalities linked to cell migration and tissue repair (Medzhitov and Horng, 2009). Intriguingly, LPS also stimulates production of inducible negative regulators, such as IκBα, that limit inflammation by interfering with proinflammatory transcription factors (Wessells et al., 2004; Kuwata et al., 2006). Negative feedback loops are broadly critical in immunity as they mitigate deleterious pathophysiological

consequences that arise from excessive inflammation. We propose that this axiom also extends to inflammatory signaling driven by sensory neurons.

Second, we establish that Arc is translated in afferent fibers in the skin. The dermis contains a diverse microenvironment that includes nerve fibers, keratinocytes, fibroblasts, nerve terminals, basal cells, capillaries, and resident immune cells. Non-neuronal cells collaborate to control the function of sensory neurons through multiple mechanisms. For example, keratinocytes facilitate detection of mechanical cues through release of ATP
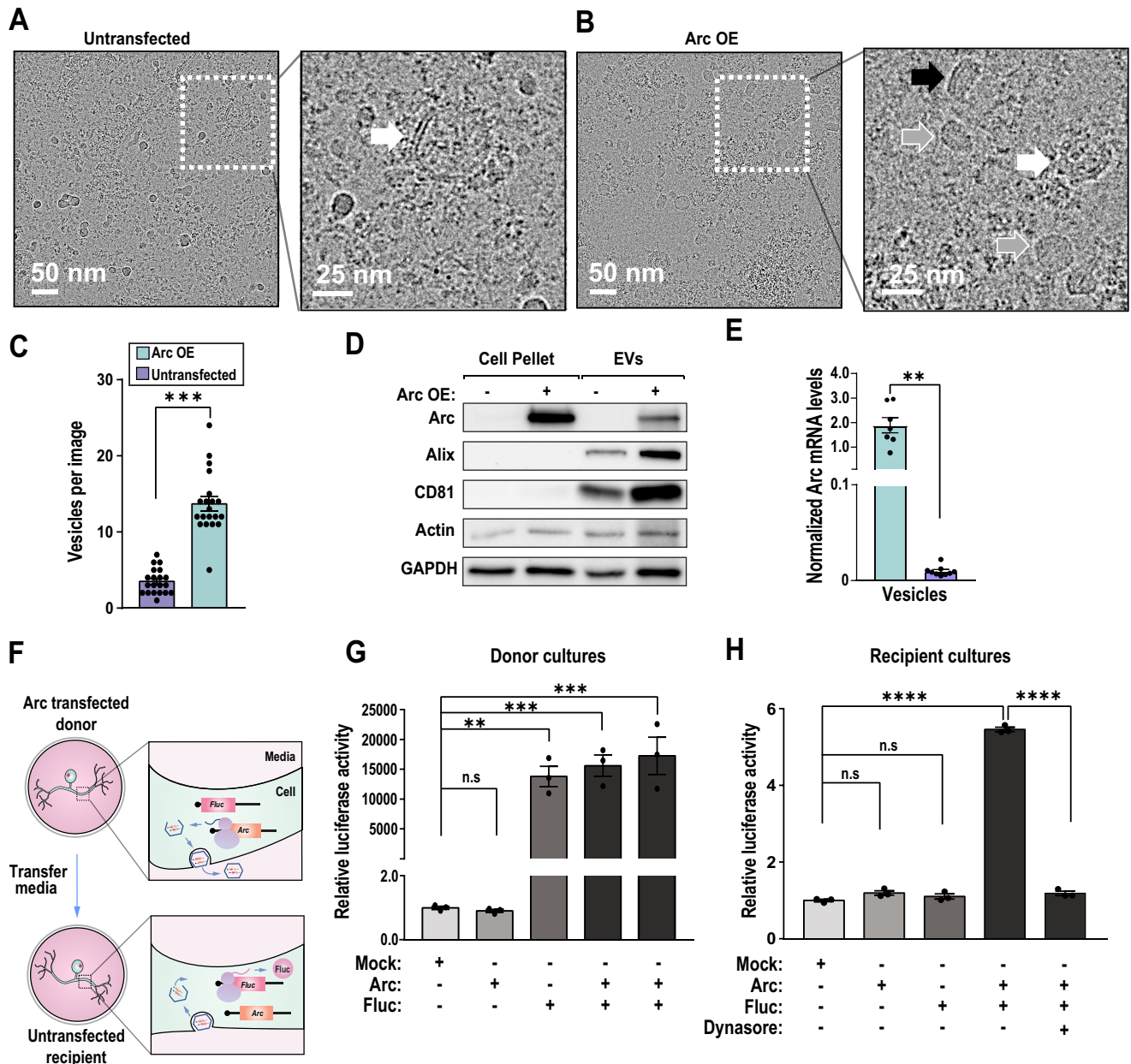
Figure 6. Sensory neurons produce *Arc*-containing EVs. **A**, left panel, Cryo-EM image of EVs purified from untransfected cells. Right panel, Closeup of region with a membrane bilayer bound vesicle (white arrow). **B**, left panel, Cryo-EM image of EVs purified from cells transfected with Arc. Right panel, Closeup on three types of vesicles that increase in abundance. After transfection the most abundant vesicle type are single membrane vesicles (gray arrow). Low-density lipoprotein (LDL)-like vesicles (black arrow), which have a characteristic striped pattern because of stacked cholesteryl esters, and bilayered vesicles (white arrow) increase in abundance as well. **C**, left panel, Average number of observed vesicles per image. A total of 20 consecutive images for each sample were evaluated. The number of EVs/image increases ~3.9-fold for the Arc transfected sample. Unpaired *t* test with Welch's correction; ***$p = 0.0003$. Size distributions are provided in Extended Data Figure 6-1. **D**, Immunoblot analysis of vesicles isolated from cells transfected with Arc are enriched for Arc, Actin, GAPDH, and vesicular markers. **E**, qPCR quantification of Arc mRNA reveals that Arc overexpression results in significant enrichment of the transcript ($n = 7$–9). Unpaired *t* test with Welch's correction; **$p = 0.0012$. **F**, A schematic depicting the model for Arc-mediated RNA transfer. Media from cells that overexpress Arc may mediate transfer of abundant mRNA species such as firefly luciferase (*Fluc*). Transfer of media from donor cells to recipient cells may result in translation of encapsulated RNAs. **G**, Firefly luciferase assay data for donor cultures normalized to a mock transfection sample. Ordinary one-way ANOVA: $F_{(4,10)} = 23$, $p \leq 0.0001$. Tukey's multiple comparisons test: mock versus Arc (not significant , n.s.), $p \geq 0.999$; mock versus Fluc, **$p = 0.0020$; mock versus Arc + Fluc (1), ***$p = 0.0003$; mock versus Arc + Fluc (2), ***$p = 0.0003$. **H**, Firefly luciferase assay data for recipient cultures normalized to a mock transfection sample. Ordinary one-way ANOVA: $F_{(4,10)} = 1220$, $p \leq 0.0001$. Tukey's multiple comparisons test: mock versus Arc (n.s.), $p = 0.1717$; mock versus Fluc (n.s.), $p = 0.6851$; mock versus Arc + Fluc, ****$p \leq 0.0001$; mock versus Arc + Fluc + dynasore (n.s.), $p = 0.2012$; Arc + Fluc versus Arc + Fluc + dynasore, ****$p \leq 0.0001$.

(Moehring et al., 2018). Immune cells secrete a range of molecules that sensitize nociceptive neurons (e.g., NGF, IL-6, PGE2, etc.; Pinho-Ribeiro et al., 2017). Communication from sensory neurons to other cell types is mediated almost exclusively by peptides. We found that Arc-deficient mice display exaggerated vasodilatation that can be rescued by injection of purified vesicles containing Arc. Based on these observations, we propose a model where

potential intercellular transport of RNA mediates communication between sensory neurons and other cell types within the dermal microenvironment. A key question moving forward will be the identification of recipient cell types that contribute to vasodilation. This could potentially be addressed through incorporation of labeled RNAs into the Arc EVs. We show that purified Arc-containing vesicles obtained from a nociceptor cell line are
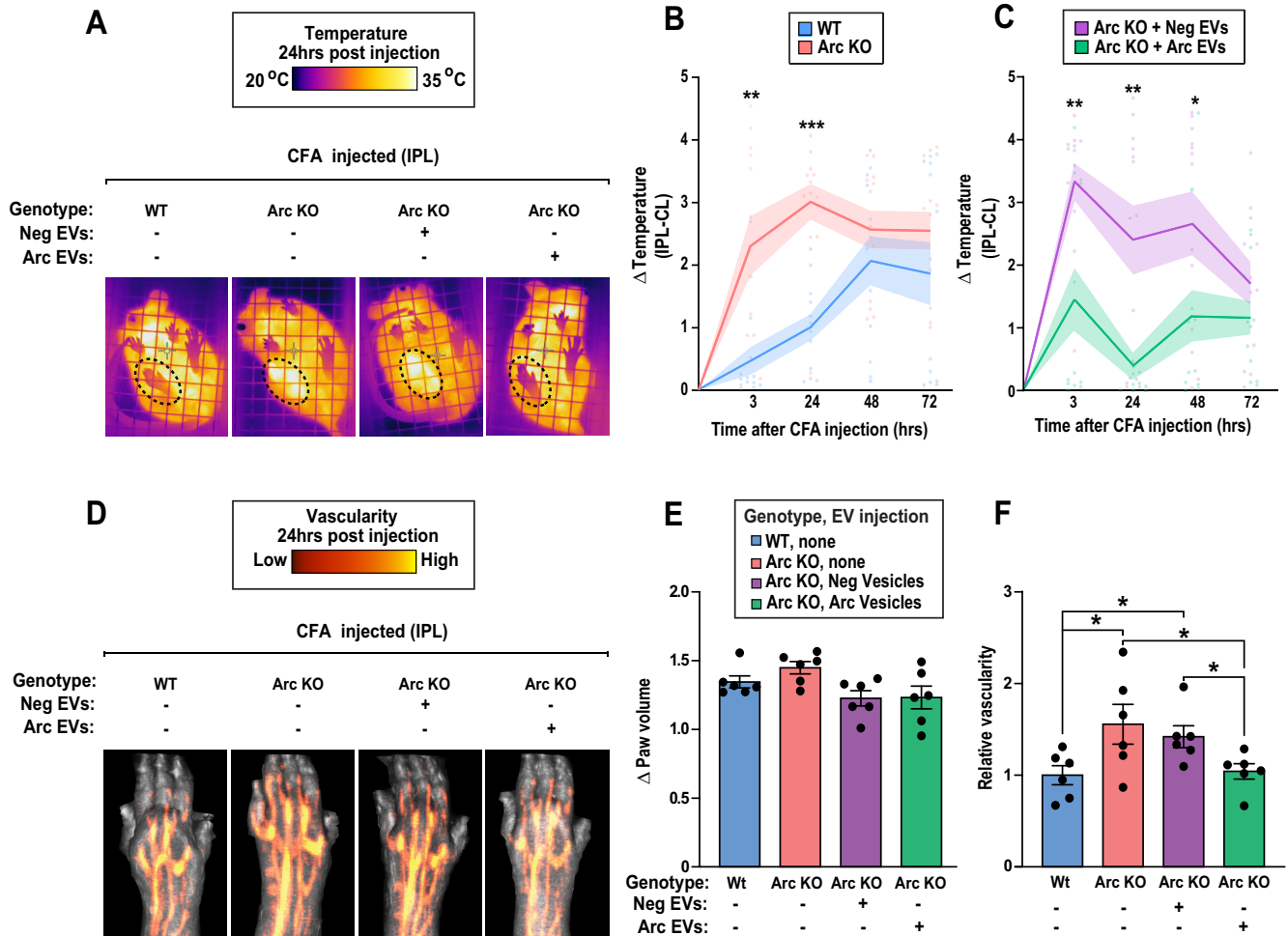
Figure 7. Arc-containing EVs reduce thermal responses and vascularity in the skin following intraplantar CFA injection. ***A***, FLIR images of the paw of wild-type (WT) and ARC KO mice after injection of 5 μg of CFA, with and without pretreatment of purified Arc vesicles (encircled paw). Arc expression in the DRG and skin of Arc KO mice and WT mice is provided in Extended Data Figure 7-1. ***B***, Arc KO mice have increased ΔTemperature than WT mice, indicating exaggerated vasodilation. Two-way ANOVA: genotype effect, $F_{(1,88)} = 25.62$, $p < 0.0001$; time effect, $F_{(3,88)} = 2.772$, $p = 0.0462$. Bonferroni's multiple comparison test: WT versus Arc KO, 3 h **$p = 0.0015$, 24 h ***$p = 0.0005$. Data are the difference in temperature between the injected (IPL) versus the uninjected (CL) paw of each mouse (ΔTemperature, °C). The thick line connects mean values and the flanking shaded areas denote SEM, $n = 12$ animals per group. ***C***, Pretreatment with purified Arc containing EVs rescues the exaggerated vasodilation in the Arc KO mice. Two-way ANOVA: vesicle effect, $F_{(1,88)} = 26.75$, $p < 0.0001$; time effect, $F_{(3,88)} = 2.720$, $p = 0.0493$. Bonferroni's multiple comparison test: WT versus Arc KO, 3 h **$p = 0.0057$, 24 h **$p = 0.0027$, 48 h *$p = 0.0458$. As in panel ***B***, the data represent change in temperature between IPL and CL paws. The thick line connects mean values and the flanking shaded areas denote SEM, $n = 12$ animals per group. ***D***, Doppler ultrasound images of the paw of WT and ARC KO mice after injection of 5 μg of CFA. Vesicle treatments were either from cells expressing Arc or Arc vesicles isolated from a transfected negative control. ***E***, Paw volumes for WT and Arc KO mice injected with CFA. Injection of EVs did not result in significant changes. Each bar represents the mean ± SEM of the change in volume between the CFA-injected and uninjected paw (ΔPaw volume); $n = 6$ animals per group. ***F***, Arc KO mice have increased vascularity than WT mice after CFA-injection, indicating exaggerated vasodilation. Pretreatment with purified Arc vesicles, but not of Neg vesicles, rescues the exaggerated vasodilation in the Arc KO mice. Unpaired t test, WT versus Arc KO *$p = 0.0432$, WT versus Arc KO + Neg EV *$p = 0.0244$, ARC KO versus ARC KO + Arc EV *$p = 0.0258$, Arc KO + Neg EV versus Arc KO + Arc EV *$p = 0.0276$. Each bar represents the mean ± SEM of the relative change in percent vascularity after CFA injection; $n = 6$ animals per group.

enriched for *Arc* mRNA. However, the vesicles likely contain multiple RNA species. While our data do not discount the possibility that the Arc protein itself could be the relevant molecule responsible for rescue, it is clearly of interest to determine the RNA content of the vesicles with the overarching goal of understanding the anti-inflammatory effects of the purified vesicles.

Third, Arc is likely translated from existing mRNA. In the brain, synaptic activity results in transcription and localization of Arc to sites of local protein synthesis (Steward et al., 1998). We found that introduction of transcriptional inhibitors did not prevent Arc accumulation in the dermis. This suggests that Arc is primarily translated from existing mRNA which departs from compelling data obtained in the rat hippocampus (Farris et al., 2014). The use of slightly different mechanisms may reflect a key anatomic challenge to local translation, distance. Sensory

neurons possess the longest axons in the body that can extend for a meter in humans. The rate an mRNA travels is at best ~5 μm/s (Park et al., 2014). Thus, a reasonable estimate for the amount of time required to transport a newly transcribed RNA a meter is 55 h. Local translation is an attractive mechanism to achieve Arc biosynthesis on demand. It is unclear how Arc is maintained in a quiescent state in fibers. One potential mechanism is through posttranslational modifications of translation factors that favor preferential patterns of translation. For example, mGluR activation stimulates rapid translation of Arc through eukaryotic elongation factor 2 kinase (eEF2K)-dependent phosphorylation of eEF2 (Park et al., 2008). This in turn reduces elongation rates of most transcripts. By an unknown mechanism, Arc evades repression by phosphorylated eEF2 in

dendrites. It would be of interest to determine whether similar regulation occurs in afferent fibers.

To summarize, translational control is prominent in sensory neurons (de la Pena et al., 2019; Loerch et al., 2019). Beyond the established role of *de novo* protein synthesis in pain associated behaviors, our experiments uncover a new target of translational regulation, Arc. We find that Arc is expressed throughout the DRG and accumulates in the skin in response to inflammatory mediators. The accumulation requires afferent fibers and is insensitive to transcriptional inhibition. We find that genetic disruption of Arc results in exaggerated inflammation that is normalized on introduction of EVs containing Arc. This suggests that Arc is a new type of anti-inflammatory mediator. Given parallel negative feedback in other systems, this is important for understanding the process of neuroinflammation. Indeed, activity-dependent vasodilation also occurs in the brain (Chow et al., 2020). However, a limitation of our data in lack of structural validation indicating the presence of Arc capsids in EVs produced by nociceptors. This information will be critical to unambiguously establish that viral-like signaling is the precise mechanism used by sensory neurons to signal to nearby cells in the dermis. Nonetheless, our data reveal a role for Arc in neuronal control of inflammation and highlight a target of induced translation in afferent fibers.

References

Afanasyev P, Ravelli RB, Matadeen R, De Carlo S, van Duinen G, Alewijnse B, Peters PJ, Abrahams JP, Portugal RV, Schatz M, van Heel M (2015) A posteriori correction of camera characteristics from large image data sets. Sci Rep 5:10317.

Andreu Z, Yáñez-Mó M (2014) Tetraspanins in extracellular vesicle formation and function. Front Immunol 5:442.

Ashley J, Cordy B, Lucia D, Fradkin LG, Budnik V, Thomson T (2018) Retrovirus-like Gag protein Arc1 binds RNA and traffics across synaptic boutons. Cell 172:262–274.e11.

Avona A, Burgos-Vega C, Burton MD, Akopian AN, Price TJ, Dussor G (2019) Dural calcitonin gene-related peptide produces female-specific responses in rodent migraine models. J Neurosci 39:4323–4331.

Bailey TL, Boden M, Buske FA, Frith M, Grant CE, Clementi L, Ren J, Li WW, Noble WS (2009) MEME SUITE: tools for motif discovery and searching. Nucleic acids Res 37:W202–W208.

Barragán-Iglesias P, Kuhn J, Vidal-Cantú GC, Salinas-Abarca AB, Granados-Soto V, Dussor GO, Campbell ZT, Price TJ (2019) Activation of the integrated stress response in nociceptors drives methylglyoxal-induced pain. Pain 160:160–171.

Bojovic O, Panja D, Bittins M, Bramham CR, Tjølsen A (2015) Time course of immediate early gene protein expression in the spinal cord following conditioning stimulation of the sciatic nerve in rats. PLoS One 10: e0123604.

Bolte S, Cordelières FP (2006) A guided tour into subcellular colocalization analysis in light microscopy. J Microsc 224:213–232.

Brain SD, Williams TJ (1989) Interactions between the tachykinins and calcitonin gene-related peptide lead to the modulation of oedema formation and blood flow in rat skin. Br J Pharmacol 97:77–82.

Butler A, Hoffman P, Smibert P, Papalexi E, Satija R (2018) Integrating single-cell transcriptomic data across different conditions, technologies, and species. Nat Biotechnol 36:411–420.

Chang DS, Hsu E, Hottinger DG, Cohen SP (2016) Anti-nerve growth factor in pain management: current evidence. J Pain Res 9:373–383.

Chiu IM, von Hehn CA, Woolf CJ (2012) Neurogenic inflammation and the peripheral nervous system in host defense and immunopathology. Nat Neurosci 15:1063–1067.

Chow BW, Nuñez V, Kaplan L, Granger AJ, Bistrong K, Zucker HL, Kumar P, Sabatini BL, Gu C (2020) Caveolae in CNS arterioles mediate neurovascular coupling. Nature 579:106–110.

De Jongh RF, Vissers KC, Meert TF, Booij LH, De Deyne CS, Heylen RJ (2003) The role of interleukin-6 in nociception and pain. Anesth Analg 96:1096–1103.

de la Pena JBI, Song JJ, Campbell ZT (2019) RNA control in pain: blame it on the messenger. Wiley Interdiscip Rev RNA 10:e1546.

Devor M, Wall PD (1981) Plasticity in the spinal cord sensory map following peripheral nerve injury in rats. J Neurosci 1:679–684.

Dubin AE, Patapoutian A (2010) Nociceptors: the sensors of the pain pathway. J Clin Invest 120:3760–3772.

Erlendsson S, Morado DR, Cullen HB, Feschotte C, Shepherd JD, Briggs JAG (2020) Structures of virus-like capsids formed by the *Drosophila* neuronal Arc proteins. Nat Neurosci 23:172–175.

Farris S, Lewandowski G, Cox CD, Steward O (2014) Selective localization of arc mRNA in dendrites involves activity- and translation-dependent mRNA degradation. J Neurosci 34:4481–4493.

Ferrari LF, Bogen O, Chu C, Levine JD (2013a) Peripheral administration of translation inhibitors reverses increased hyperalgesia in a model of chronic pain in the rat. J Pain 14:731–738.

Ferrari LF, Bogen O, Levine JD (2013b) Role of nociceptor αCaMKII in transition from acute to chronic pain (hyperalgesic priming) in male and female rats. J Neurosci 33:11002–11011.

Ferrari LF, Araldi D, Levine JD (2015) Distinct terminal and cell body mechanisms in the nociceptor mediate hyperalgesic priming. J Neurosci 35:6107–6116.

Gibson DG, Young L, Chuang RY, Venter JC, Hutchison CA, Smith HO (2009) Enzymatic assembly of DNA molecules up to several hundred kilobases. Nat Methods 6:343–345.

Glusman G, Caballero J, Robinson M, Kutlu B, Hood L (2013) Optimal scaling of digital transcriptomes. PLoS One 8:e77885.

Grant T, Rohou A, Grigorieff N (2018) cisTEM, user-friendly software for single-particle image processing. Elife 7:e35383.

Guenthner CJ, Miyamichi K, Yang HH, Heller HC, Luo L (2013) Permanent genetic access to transiently active neurons via TRAP: targeted recombination in active populations. Neuron 78:773–784.

Guzowski JF, McNaughton BL, Barnes CA, Worley PF (1999) Environment-specific expression of the immediate-early gene Arc in hippocampal neuronal ensembles. Nat Neurosci 2:1120–1124.

Guzowski JF, Lyford GL, Stevenson GD, Houston FP, McGaugh JL, Worley PF, Barnes CA (2000) Inhibition of activity-dependent arc protein expression in the rat hippocampus impairs the maintenance of long-term potentiation and the consolidation of long-term memory. J Neurosci 20:3993–4001.

Hornstein N, Torres D, Das Sharma S, Tang G, Canoll P, Sims PA (2016) Ligation-free ribosome profiling of cell type-specific translation in the brain. Genome Biol 17:149.

Hossaini M, Jongen JL, Biesheuvel K, Kuhl D, Holstege JC (2010) Nociceptive stimulation induces expression of Arc/Arg3.1 in the spinal cord with a preference for neurons containing enkephalin. Mol Pain 6:43.

Hsieh AC, Liu Y, Edlind MP, Ingolia NT, Janes MR, Sher A, Shi EY, Stumpf CR, Christensen C, Bonham MJ, Wang S, Ren P, Martin M, Jessen K, Feldman ME, Weissman JS, Shokat KM, Rommel C, Ruggero D (2012) The translational landscape of mTOR signalling steers cancer initiation and metastasis. Nature 485:55–61.

Ingolia NT (2010) Genome-wide translational profiling by ribosome footprinting. Methods Enzymol 470:119–142.

Kedrov AV, Durymanov M, Anokhin KV (2019) The Arc gene: retroviral heritage in cognitive functions. Neurosci Biobehav Rev 99:275–281.

Kuleshov MV, Jones MR, Rouillard AD, Fernandez NF, Duan Q, Wang Z, Koplev S, Jenkins SL, Jagodnik KM, Lachmann A, McDermott MG, Monteiro CD, Gundersen GW, Ma'ayan A (2016) Enrichr: a comprehensive gene set enrichment analysis web server 2016 update. Nucleic Acids Res 44:W90–W97.

Kuwata H, Matsumoto M, Atarashi K, Morishita H, Hirotani T, Koga R, Takeda K (2006) IkappaBNS inhibits induction of a subset of Toll-like receptor-dependent genes and limits inflammation. Immunity 24:41–51.

Li CL, Li KC, Wu D, Chen Y, Luo H, Zhao JR, Wang SS, Sun MM, Lu YJ, Zhong YQ, Hu XY, Hou R, Zhou BB, Bao L, Xiao HS, Zhang X (2016) Somatosensory neuron types identified by high-coverage single-cell RNA-sequencing and functional heterogeneity. Cell Res 26:83–102.

Link W, Konietzko U, Kauselmann G, Krug M, Schwanke B, Frey U, Kuhl D (1995) Somatodendritic expression of an immediate early gene is regulated by synaptic activity. Proc Natl Acad Sci USA 92:5734–5738.

Loerch S, De la Peña JB, Song Pancrazio JJJ, Price TJ, Campbell ZT (2019) Translational controls in pain. In: The Oxford handbook of neuronal

protein synthesis (Sossin W, ed), pp 1–26. Oxford: Oxford University Press.

Lyford GL, Yamagata K, Kaufmann WE, Barnes CA, Sanders LK, Copeland NG, Gilbert DJ, Jenkins NA, Lanahan AA, Worley PF (1995) Arc, a growth factor and activity-regulated gene, encodes a novel cytoskeleton-associated protein that is enriched in neuronal dendrites. Neuron 14:433–445.

Mastronarde DN (2005) Automated electron microscope tomography using robust prediction of specimen movements. J Struct Biol 152:36–51.

McIntyre CK, Miyashita T, Setlow B, Marjon KD, Steward O, Guzowski JF, McGaugh JL (2005) Memory-influencing intra-basolateral amygdala drug infusions modulate expression of Arc protein in the hippocampus. Proc Natl Acad Sci USA 102:10718–10723.

Medzhitov R, Horng T (2009) Transcriptional control of the inflammatory response. Nat Rev Immunol 9:692–703.

Megat S, Ray PR, Moy JK, Lou TF, Barragán-Iglesias P, Li Y, Pradhan G, Wanghzou A, Ahmad A, Burton MD, North RY, Dougherty PM, Khoutorsky A, Sonenberg N, Webster KR, Dussor G, Campbell ZT, Price TJ (2019) Nociceptor translational profiling reveals the ragulator-Rag GTPase complex as a critical generator of neuropathic pain. J Neurosci 39:393–411.

Melemedjian OK, Asiedu MN, Tillu DV, Peebles KA, Yan J, Ertz N, Dussor GO, Price TJ (2010) IL-6- and NGF-induced rapid control of protein synthesis and nociceptive plasticity via convergent signaling to the eIF4F complex. J Neurosci 30:15113–15123.

Minatohara K, Akiyoshi M, Okuno H (2015) Role of immediate-early genes in synaptic plasticity and neuronal ensembles underlying the memory trace. Front Mol Neurosci 8:78.

Moehring F, Cowie AM, Menzel AD, Weyer AD, Grzybowski M, Arzua T, Geurts AM, Palygin O, Stucky CL (2018) Keratinocytes mediate innocuous and noxious touch via ATP-P2X4 signaling. Elife 7:e31684.

Moll P, Ante M, Seitz A, Reda T (2014) QuantSeq 3′ mRNA sequencing for RNA quantification. Nat Methods 11:i–iii.

Moy JK, Khoutorsky A, Asiedu MN, Black BJ, Kuhn JL, Barragán-Iglesias P, Megat S, Burton MD, Burgos-Vega CC, Melemedjian OK, Boitano S, Vagner J, Gkogkas CG, Pancrazio JJ, Mogil JS, Dussor G, Sonenberg N, Price TJ (2017) The MNK–eIF4E signaling axis contributes to injury-induced nociceptive plasticity and the development of chronic pain. J Neurosci 37:7481–7499.

Obreja O, Rukwied R, Nagler L, Schmidt M, Schmelz M, Namer B (2018) Nerve growth factor locally sensitizes nociceptors in human skin. Pain 159:416–426.

Okuno H, Akashi K, Ishii Y, Yagishita-Kyo N, Suzuki K, Nonaka M, Kawashima T, Fujii H, Takemoto-Kimura S, Abe M, Natsume R, Chowdhury S, Sakimura K, Worley PF, Bito H (2012) Inverse synaptic tagging of inactive synapses via dynamic interaction of Arc/Arg3.1 with CaMKIIβ. Cell 149:886–898.

Park HY, Lim H, Yoon YJ, Follenzi A, Nwokafor C, Lopez-Jones M, Meng X, Singer RH (2014) Visualization of dynamics of single endogenous mRNA labeled in live mouse. Science 343:422–424.

Park S, Park JM, Kim S, Kim JA, Shepherd JD, Smith-Hicks CL, Chowdhury S, Kaufmann W, Kuhl D, Ryazanov AG, Huganir RL, Linden DJ, Worley PF (2008) Elongation factor 2 and fragile X mental retardation protein control the dynamic translation of Arc/Arg3.1 essential for mGluR-LTD. Neuron 59:70–83.

Pastuzyn ED, Day CE, Kearns RB, Kyrke-Smith M, Taibi AV, McCormick J, Yoder N, Belnap DM, Erlendsson S, Morado DR, Briggs JAG, Feschotte C, Shepherd JD (2018) The neuronal gene Arc encodes a repurposed retrotransposon Gag protein that mediates intercellular RNA transfer. Cell 173:275.

Pinho-Ribeiro FA, Verri WA, Chiu IM (2017) Nociceptor sensory neuron-immune interactions in pain and inflammation. Trends Immunol 38:5–19.

Plath N, Ohana O, Dammermann B, Errington ML, Schmitz D, Gross C, Mao X, Engelsberg A, Mahlke C, Welzl H, Kobalz U, Stawrakakis A, Fernandez E, Waltereit R, Bick-Sander A, Therstappen E, Cooke SF,

Blanquet V, Wurst W, Salmen B, et al. (2006) Arc/Arg3.1 is essential for the consolidation of synaptic plasticity and memories. Neuron 52:437–444.

Platika D, Boulos MH, Baizer L, Fishman MC (1985) Neuronal traits of clonal cell lines derived by fusion of dorsal root ganglia neurons with neuroblastoma cells. Proc Natl Acad Sci USA 82:3499–3503.

Richardson JD, Vasko MR (2002) Cellular mechanisms of neurogenic inflammation. J Pharmacol Exp Ther 302:839–845.

Rosen JB, Fanselow MS, Young SL, Sitcoske M, Maren S (1998) Immediate-early gene expression in the amygdala following footshock stress and contextual fear conditioning. Brain Res 796:132–142.

Safieh-Garabedian B, Poole S, Allchorne A, Winter J, Woolf CJ (1995) Contribution of interleukin-1 beta to the inflammation-induced increase in nerve growth factor levels and inflammatory hyperalgesia. Br J Pharmacol 115:1265–1275.

Saria A (1984) Substance P in sensory nerve fibres contributes to the development of oedema in the rat hind paw after thermal injury. Br J Pharmacol 82:217–222.

Shepherd JD, Bear MF (2011) New views of Arc, a master regulator of synaptic plasticity. Nat Neurosci 14:279–284.

Steward O, Wallace CS, Lyford GL, Worley PF (1998) Synaptic activation causes the mRNA for the IEG Arc to localize selectively near activated postsynaptic sites on dendrites. Neuron 21:741–751.

Steward O, M Yee K, Farris S, Pirbhoy PS, Worley P, Okamura K, Okuno H, Bito H (2017) Delayed degradation and impaired dendritic delivery of intron-lacking EGFP-Arc/Arg3.1 mRNA in EGFP-Arc transgenic mice. Front Mol Neurosci 10:435.

Su TF, Zhao YQ, Zhang LH, Peng M, Wu CH, Pei L, Tian B, Zhang J, Shi J, Pan HL, Li M (2012) Electroacupuncture reduces the expression of proinflammatory cytokines in inflamed skin tissues through activation of cannabinoid CB2 receptors. Eur J Pain 16:624–635.

Svensson CI (2010) Interleukin-6: a local pain trigger? Arthritis Res Ther 12:145.

Tanda G (2015) The use of infrared thermography to detect the skin temperature response to physical activity. J Phys Conf Ser 655.

Tandrup T, Woolf CJ, Coggeshall RE (2000) Delayed loss of small dorsal root ganglion cells after transection of the rat sciatic nerve. J Comp Neurol 422:172–180.

Toda M, Suzuki T, Hosono K, Hayashi I, Hashiba S, Onuma Y, Amano H, Kurihara Y, Kurihara H, Okamoto H, Hoka S, Majima M (2008) Neuronal system-dependent facilitation of tumor angiogenesis and tumor growth by calcitonin gene-related peptide. Proc Natl Acad Sci USA 105:13550–13555.

Ufer F, Vargas P, Engler JB, Tintelnot J, Schattling B, Winkler H, Bauer S, Kursawe N, Willing A, Keminer O, Ohana O, Salinas-Riester G, Pless O, Kuhl D, Friese MA (2016) Arc/Arg3.1 governs inflammatory dendritic cell migration from the skin and thereby controls T cell activation. Sci Immunol 1:eaaf8665.

Uttam S, Wong C, Amorim IS, Jafarnejad SM, Tansley SN, Yang J, Prager-Khoutorsky M, Mogil JS, Gkogkas CG, Khoutorsky A (2018) Translational profiling of dorsal root ganglia and spinal cord in a mouse model of neuropathic pain. Neurobiol Pain 4:35–44.

Van der Maaten L, Hinton G (2008) Visualizing data using t-SNE. J Mach Learn Res 9:2579–2605.

Vann SD, Brown MW, Erichsen JT, Aggleton JP (2000) Fos imaging reveals differential patterns of hippocampal and parahippocampal subfield activation in rats in response to different spatial memory tests. J Neurosci 20:2711–2718.

Wessells J, Baer M, Young HA, Claudio E, Brown K, Siebenlist U, Johnson PF (2004) BCL-3 and NF-kappaB p50 attenuate lipopolysaccharide-induced inflammatory responses in macrophages. J Biol Chem 279:49995–50003.

Willms E, Cabanas C, Mager I, Wood MJA, Vader P (2018) Extracellular vesicle heterogeneity: subpopulations, isolation techniques, and diverse functions in cancer progression. Front Immunol 9:738.